

# JGR Biogeosciences

## RESEARCH ARTICLE

10.1029/2019JG005474

### Key Points:

- Reservoirs are the fourth largest anthropogenic methane source in the U.S. state of Ohio
- Variables in national databases (reservoir size) predict methane emission rates nearly as well as variables measured on-site (nutrients)
- The global warming potential of methane emissions from reservoirs exceeded that of carbon dioxide emissions

### Supporting Information:

- Supporting Information S1

### Correspondence to:

J. J. Beaulieu,  
beaulieu.jake@epa.gov

### Citation:

Beaulieu, J. J., Waldo, S., Balz, D. A., Barnett, W., Hall, A., Platz, M. C., & White, K. M. (2020). Methane and carbon dioxide emissions from reservoirs: Controls and upscaling. *Journal of Geophysical Research: Biogeosciences*, 125, e2019JG005474. <https://doi.org/10.1029/2019JG005474>

Received 20 SEP 2019

Accepted 24 AUG 2020

Accepted article online 15 OCT 2020

## Methane and Carbon Dioxide Emissions From Reservoirs: Controls and Upscaling

Jake J. Beaulieu<sup>1</sup> , Sarah Waldo<sup>1</sup> , David A. Balz<sup>2</sup>, Will Barnett<sup>3</sup>, Alexander Hall<sup>1</sup> , Michelle C. Platz<sup>4</sup> , and Karen M. White<sup>1</sup>

<sup>1</sup>United States Environmental Protection Agency, Office of Research and Development, Cincinnati, OH, USA, <sup>2</sup>Pegasus Technical Services, Cincinnati, OH, USA, <sup>3</sup>Neptune Inc, Lakewood, CO, USA, <sup>4</sup>Department of Civil and Environmental Engineering, University of South Florida, Tampa, FL, USA

**Abstract** Estimating carbon dioxide (CO<sub>2</sub>) and methane (CH<sub>4</sub>) emission rates from reservoirs is important for regional and national greenhouse gas inventories. A lack of methodologically consistent data sets for many parts of the world, including agriculturally intensive areas of the United States, poses a major challenge to the development of models for predicting emission rates. In this study, we used a systematic approach to measure CO<sub>2</sub> and CH<sub>4</sub> diffusive and ebullitive emission rates from 32 reservoirs distributed across an agricultural to forested land use gradient in the United States. We found that all reservoirs were a source of CH<sub>4</sub> to the atmosphere, with ebullition being the dominant emission pathway in 75% of the systems. Ebullition was a negligible emission pathway for CO<sub>2</sub>, and 65% of sampled reservoirs were a net CO<sub>2</sub> sink. Boosted regression trees (BRTs), a type of machine learning algorithm, identified reservoir morphology and watershed agricultural land use as important predictors of emission rates. We used the BRT to predict CH<sub>4</sub> emission rates for reservoirs in the U.S. state of Ohio and estimate they are the fourth largest anthropogenic CH<sub>4</sub> source in the state. Our work demonstrates that CH<sub>4</sub> emission rates for reservoirs in our study region can be predicted from information in readily available national geodatabases. Expanded sampling campaigns could generate the data needed to train models for upscaling in other U.S. regions or nationally.

## 1. Introduction

Lakes and reservoirs are sites of intense carbon processing in the landscape. Carbon that enters lentic ecosystems through watershed runoff or internal primary production is subject to microbial transformations, often resulting in the production of the greenhouse gases (GHGs) carbon dioxide (CO<sub>2</sub>) and methane (CH<sub>4</sub>). It is estimated that lentic waters emit between 110 and 810 Tg CO<sub>2</sub>-C (Cole et al., 2007; DelSontro et al., 2018; Tranvik et al., 2009) and 69–112 Tg CH<sub>4</sub>-C (Bastviken et al., 2011; DelSontro et al., 2018) to the atmosphere each year, equivalent to roughly 20% of global CO<sub>2</sub> fossil fuel emission.

Emissions from reservoirs are of particular interest due to the complex tradeoffs between the societal services provided by reservoirs (i.e., hydropower, shipping, drinking water) and their environmental impact. Reservoirs have been recognized as sources of CO<sub>2</sub> and CH<sub>4</sub> since the early 90s (Rudd et al., 1993) and the World Bank, UNESCO, and International Hydropower Association encourage assessments of potential GHG emissions when planning dam infrastructure projects (International Hydropower Association, 2010; Liden, 2013; Prairie et al., 2017). Furthermore, under the Intergovernmental Panel on Climate Change (IPCC) GHG reporting framework, emissions from reservoirs are considered “anthropogenic” and can be included in a nation’s GHG inventory reported to the IPCC under the United Nations Framework Convention on Climate Change treaty, whereas emissions from lakes are considered “natural” and therefore cannot be included in the GHG inventory. While the distinction between “natural” and “anthropogenic” emissions is an oversimplification, it has led to increased interest in quantifying GHG emissions from reservoirs.

The recently adopted IPCC methodology (Lovelock et al., 2019) for estimating reservoir CO<sub>2</sub> and CH<sub>4</sub> emissions provides average emission rates (aka emission factors) for six major climate zones, but countries may choose to develop country specific emission factors or models, particularly where reservoirs constitute an important proportion of anthropogenic CH<sub>4</sub> and/or CO<sub>2</sub> emissions. Although earlier studies suggested

that tropical reservoirs had higher CH<sub>4</sub> emission rates than temperate systems (Barros et al., 2011), a more recent data synthesis found little evidence for differences in emission rates among climate zones (Deemer et al., 2016), due partly to recent reports of high emission rates from eutrophic reservoirs in the United States and Switzerland (Beaulieu et al., 2014, 2016, 2018; DelSontro et al., 2010). Beaulieu et al. (2014) estimated that CH<sub>4</sub> emissions from reservoirs draining watersheds managed for corn and soybean production in the United States may emit 2.2 Tg CH<sub>4</sub>-C y<sup>-1</sup>, equivalent to 10% of the nation's annual anthropogenic CH<sub>4</sub> emissions. This estimate was derived by extrapolating measurements made at one agricultural reservoir to all U.S. agricultural reservoirs and is therefore highly uncertain, but suggests that reservoirs may be an important component of the U.S. anthropogenic CH<sub>4</sub> inventory.

Most attempts to upscale GHG emission rates from individual waterbodies to regional or global estimates simply multiply an average emission rate by the total waterbody surface area in the region of interest (Barros et al., 2011; Bastviken et al., 2011; Cole et al., 2007; St. Louis et al., 2000; Tranvik et al., 2009). This upscaling approach can be highly biased, however, unless the emission rate measurements come from a representative sample of lakes or reservoirs in the region of interest, which is unlikely. Most investigators choose sites based on convenience, the presence of research infrastructure, or other unique features. This set of criteria is unlikely to generate a collection of published emission rates that are representative of the population of lakes or reservoirs in the region. An alternative upscaling approach is to use published emission rate data to parameterize a statistical model relating emission rates to important drivers. Assuming the statistical relationships derived from the sample are applicable to the population, the model can be used to predict emission rates based on information about the population of lakes and reservoirs. In this approach, the sample data should come from waterbodies that cover a sufficiently large range of values for the explanatory variables but do not need to be a representative sample of the population of interest. For example, DelSontro et al. (2018) built statistical models relating CH<sub>4</sub>, CO<sub>2</sub>, and N<sub>2</sub>O emission rates to measures of productivity (e.g., chlorophyll *a* [chl *a*] and total phosphorus) and lake size. These models were then used to predict emission rates across the globe based on satellite derived measures of chl *a* and published lake size distributions.

Predicting emission rates from models is only possible if information about the model drivers is known at unsampled locations. Historically, this has been a major impediment to upscaling, but advances in remote sensing and geospatial modeling are beginning to address this. For example, the LakeCat database (Hill et al., 2018) contains 136 metrics describing watershed conditions (e.g., size and land use) for 378,088 waterbodies in the conterminous United States and the LakeMorpho database (Hollister et al., 2011; Hollister & Stachelek, 2018) contains information on morphometry (e.g., surface area and mean depth) for 363,314 waterbodies in the conterminous United States.

Another limitation to upscaling reservoir GHG emissions in the United States is a relative lack of published measurements. For example, total CH<sub>4</sub> emission rates (diffusive + ebullitive) for U.S. reservoirs are only available for one reservoir in Ohio (Beaulieu et al., 2014, 2016, 2018), six reservoirs in the southeastern United States (Bevelhimer et al., 2016), and six reservoirs in the Pacific Northwest (Harrison et al., 2017). Furthermore, the spatial and temporal resolution of the measurements varies among studies, complicating direct comparison of published rates.

The objectives of this work are to (1) identify important environmental drivers of CO<sub>2</sub> and CH<sub>4</sub> emission rates from reservoirs in the midwestern United States, (2) upscale the measured emission rates to all reservoirs in one state in the region, and (3) test the model predictions against published emission rate measurements from other parts of the country. To achieve these objectives, we used a statistical survey design and consistent methodology to measure CH<sub>4</sub> and CO<sub>2</sub> emission rates from 32 reservoirs in Ohio, Kentucky, and Indiana. Emission rates were modeled using driver data collected from LakeCat, LakeMorpho, and on-site measurements (e.g., chl and total phosphorus). We show that reservoir emission rates can be predicted from driver data contained in national databases and that there is little improvement in prediction accuracy when on-site measurements are included in the model. When upscaled to the U.S. state of Ohio, we found that reservoirs are the fourth largest anthropogenic CH<sub>4</sub> source. We also demonstrate that the model performs poorly when used to predict emission rates outside of the study region, suggesting that controls on reservoir GHG emission rates may vary by region.

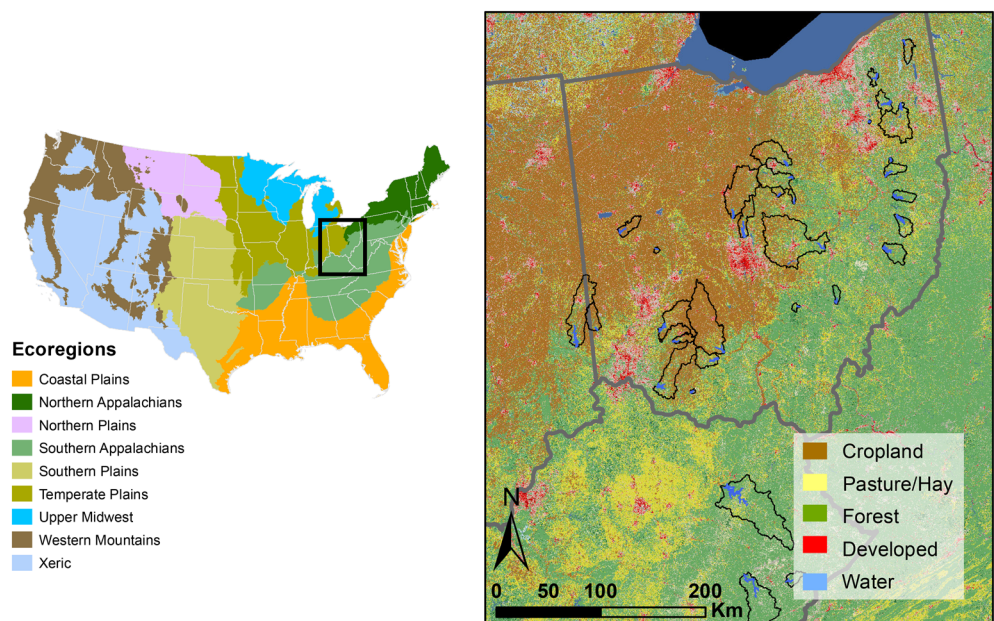


**Figure 1.** Site map illustrating major U.S. ecoregions and location of 32 sampled reservoirs in study area. Reservoir surface area is shown in blue, and watershed boundaries are delineated in black.

## 2. Methods

### 2.1. Site Selection and Survey Design

The survey was designed to include reservoirs that spanned a range of depth and watershed land use conditions, two factors which can have a strong effect on  $\text{CH}_4$  dynamics. Candidate sample sites included the Ohio reservoirs in the National Inventory of Dams (NID) (United States Army Corps of Engineers, 2013) and the 21 reservoirs in the U.S. Army Corps of Engineers (USACE) Louisville District. Reservoirs determined to be industrial waste ponds, offstream ponds, or part of a series of reservoirs closely arrayed along a single river channel were omitted, leaving a total of 73 candidate reservoirs. Watershed land use was characterized for each candidate reservoir using 2011 NLCD data (U.S. Geological Survey, 2014) and maximum reservoir depth was determined from bathymetric maps. Each reservoir was placed into one of 16 groups representing unique combinations of four agricultural land use levels, based on the quartiles of the agricultural land use distribution, and four maximum depth levels, also based on the quartiles of maximum depth distribution. Two reservoirs were selected from each of the 16 groups, resulting in 32 reservoirs distributed across Ohio, Kentucky, and Indiana (Figure 1). This design resulted in a balanced complement of shallow and deep reservoirs across the agriculture to forested land use gradient in this three-state region. Each reservoir was sampled during a single contiguous 2-day period between 1 June and 14 September 2016, except for Acton Lake which was also sampled on three dates in 2017 (Table S1 in the supporting information). The sampling dates were chosen to reflect warm season conditions when waterbodies were stratified and  $\text{CH}_4$  production rates were high.

A generalized random tessellation survey (GRTS) design (Olsen et al., 2012) was established for each of the 32 reservoirs using the *spsurvey* package (Kincaid & Olsen, 2015) in R (R Development Core Team, 2016). The GRTS design included a minimum of 15 sampling sites per reservoir, with up to 27 sites in the largest reservoir. To increase the accuracy and precision of the reservoir-scale emission rate estimates, areas immediately below the largest tributary inputs, where emission rates are often high and spatially variable (Beaulieu et al., 2014, 2016), were sampled at a higher density than open-water portions of the reservoir. This stratification scheme was employed in 27 reservoirs with distinct “tributary” and “open-water” areas. Point estimates were scaled to population level estimates of mean and variance using an approach based on the Horvitz–Thompson theorem as described in Stevens and Olsen (2003) and implemented in *spsurvey*. Population level estimates from the four Acton Lake surveys were aggregated into a single estimate of mean and variance for the reservoir. Differences in emission rates among strata (open water and tributary) within

individual waterbodies were assessed by comparing the 95% confidence interval of the estimate for each stratum.

## 2.2. Measurements

Ebullitive and diffusive CO<sub>2</sub> and CH<sub>4</sub> emission rates were measured at all sites. Water temperature, dissolved oxygen (DO), specific conductivity, pH, and chl were measured at a depth of 0.2 m below the water surface at all sites and 0.5 m above the sediment-water interface at the shallowest site. These parameters were also measured at 1 m depth intervals throughout the water column at the deepest site in each reservoir. Water samples were collected from 0.2 m depth for total nitrogen (TN), total phosphorus (TP), total organic carbon (TOC), dissolved CH<sub>4</sub>, and dissolved CO<sub>2</sub> at the deepest and shallowest sites. Barometric pressure was measured at the deepest and shallowest sites in each reservoir.

One reservoir from the survey, Acton Lake, was selected for additional measurements. An inverted funnel (described below) was deployed at a shallow (1.5 m) and deep (12 m) site at Acton Lake from 15 May to 10 December in 2016 and 2017. Gas was collected from the traps every 2 weeks and analyzed for CH<sub>4</sub> and N<sub>2</sub> content.

## 2.3. Emission Rates

Short term floating chamber deployments were used to measure diffusive CO<sub>2</sub> and CH<sub>4</sub> emission rates (CO<sub>2</sub>-D and CH<sub>4</sub>-D, respectively). The dimensions of the aluminum chamber were identical to those of the CSIRO chamber presented in Zhao et al. (2015). The chamber floated on foam filled PVC pontoons with the chamber walls approximately 2.5 cm below the water surface. The headspace was mixed with a 0.658 m<sup>3</sup>/min fan and vented through 0.48 cm i.d. × 12 m tubing to equilibrate the internal headspace pressure with the atmosphere. The tubing was sufficiently long to assure no gas exchange between the chamber headspace and atmosphere. The chamber headspace was interfaced to a DC operated gas analyzer (Ultra Portable Greenhouse Gas analyzer, Los Gatos Research, San Jose, CA, USA) via 0.32 cm i.d. tubing. The analyzer continuously recirculated the chamber headspace during each 5 min deployment and recorded H<sub>2</sub>O, CH<sub>4</sub>, and CO<sub>2</sub> partial pressure every 5 s. A 10-point calibration curve was established at the beginning of the field season and verified at the end of the field season, and a one-point calibration check was performed in the field prior to each deployment.

Diffusive emission rates were calculated as

$$\text{CH}_4\text{-D or CO}_2\text{-D} = (\Delta c / \Delta t)(V/A)(P/RT)$$

where  $\Delta c / \Delta t$  is the rate of change (ppmv h<sup>-1</sup>) of CH<sub>4</sub> or CO<sub>2</sub> in the chamber headspace,  $V$  is the chamber volume (L),  $A$  is the area of the water surface enclosed by the chamber (m<sup>2</sup>),  $P$  is the pressure (atm) inside the chamber (assumed to be equal to atmospheric pressure),  $R$  is the universal gas constant, and  $T$  is the air temperature (K). Diffusive emission rates were converted from mol m<sup>-2</sup> d<sup>-1</sup> to mg m<sup>-2</sup> d<sup>-1</sup> using the molecular weight of CO<sub>2</sub> or CH<sub>4</sub>.

The CO<sub>2</sub> and CH<sub>4</sub> rate of change in the chamber headspace was quantified using a linear and nonlinear model. The linear model assumes a constant emission rate during the deployment, whereas the nonlinear model assumes a decreasing emission rate as the concentration gradient between the dissolved gas and the chamber headspace diminishes during the deployment (Stolk et al., 2009). The nonlinear model is of the form

$$c_t = c_{\max} - [(c_{\max} - c_0)\exp(-Kt)]$$

where  $c_{\max}$  (ppm) is the maximum concentration that can be reached in the chamber,  $c_0$  (ppm) is the initial concentration,  $t$  is time, and  $K$  (min<sup>-1</sup>) is a rate constant (Demello & Hines, 1994; Stolk et al., 2009). The model was fit to the data using nonlinear least squares in the minpack.lm package (Elzhov et al., 2016) and the rate of change of CO<sub>2</sub> and CH<sub>4</sub> in the chamber headspace at  $t = 0$  is calculated as

$$\Delta c / \Delta t = K (c_{\max} - c_0)$$

The acceptance criteria for model fits was a coefficient of determination ( $r^2$ ) of >0.9 and the model best supported by the data was chosen using Akaike information criterion (AIC).



Ebullitive emission rates ( $\text{CO}_2\text{-E}$  or  $\text{CH}_4\text{-E}$ ;  $\text{mg m}^{-2} \text{h}^{-1}$ ) were measured using 0.56 m diameter inverted funnels suspended 0.8 m below an anchored buoy and topped with a gas collection reservoir equipped with a ball valve and luer lock fitting. Funnels were deployed between 10:00 and 21:00 (median deployment time = 14:44) and retrieved between 07:30 and 17:00 (median retrieval time = 10:28), for a median deployment duration of 19.4 h (min = 14.5 h, max = 28.5 h). Upon retrieval, the total volume of gas in the collection reservoir was measured using graduated polypropylene syringes and up to three 20 ml samples were transferred to preevacuated ( $<50$  mTorr) 12 ml glass vials (Exetainers, LabCo, Wales, U.K.) equipped with a PTFE silicone septa stacked on top of a chlorobutyl rubber septa and analyzed for  $\text{CH}_4$ ,  $\text{CO}_2$ , and  $\text{N}_2$  partial pressure.

Ebullitive emission rates were calculated by multiplying the volumetric ebullition rate ( $\text{ml m}^{-2} \text{h}^{-1}$ ) by the molar volume at the lake temperature ( $\text{mol L}^{-1}$ ) and the fraction of  $\text{CH}_4$  or  $\text{CO}_2$  in the bubble gas. Finally, the molar ebullitive flux rate ( $\text{mole m}^{-2} \text{h}^{-1}$ ) was converted to a mass flux ( $\text{mg C m}^{-2} \text{h}^{-1}$ ). Total emission rates ( $\text{CO}_2\text{-T}$  or  $\text{CH}_4\text{-T}$ ) were calculated as the sum of diffusion and ebullition.

To determine the net GHG footprint of the reservoirs,  $\text{CH}_4$  emission rates were converted to  $\text{CO}_2$ -equivalents ( $\text{CO}_2\text{-eq}$ ) using a 100-year time horizon Global Warming Potential (GWP) of 34 (Stocker et al., 2013). Due to their different lifetimes in the atmosphere, the warming potential of  $\text{CH}_4$  relative to  $\text{CO}_2$  depends on the timescale of interest and the IPCC provides different GWP values for 20-, 100-, and 500-year time horizons. Over time the C dynamics of flooded ecosystems tend to shift (Prairie et al., 2017), calling into question the use of GWP for short-term studies (Frolking et al., 2006). We chose to use the 100-year time horizon for several reasons: (1) life-cycle analysis studies often assume a reservoir lifetime of 100 years (e.g., Gagnon et al., 2002; Prairie, Alm, Beaulieu, et al., 2017), (2) to be consistent with the method used in the USEPA's National Inventory of Greenhouse Gas Sources and Sinks (US Environmental Protection Agency, 2019b), and (3) to be consistent with many other published studies (e.g., Deemer et al., 2016; DelSontro et al., 2018).

#### 2.4. Environmental Variables

Duplicate dissolved gas samples were collected by pulling 115 ml of water into a 140 ml polypropylene syringe containing 25 ml of air and fitted with a two-way stopcock. The stopcock was closed underwater, then the syringe was gently shaken for 5 min to equilibrate the gas and water phases. After equilibration, a 27 gage needle was attached to the stopcock and flushed with 5 ml of equilibrated gas. The remaining 20 ml of equilibrated gas was transferred to a preevacuated ( $<50$  mTorr) 12 ml glass vial (Exetainers, LabCo, Wales, U.K.). Triplicate 20 ml air samples were collected in 30 ml polypropylene syringes from 2.5 m above the water surface and transferred to preevacuated 12 ml glass vials. The dissolved  $\text{CO}_2$  and  $\text{CH}_4$  concentration in the original water sample was calculated from the Bunsen solubility coefficient at the temperature of the headspace equilibration, an assumed  $\text{CO}_2$  and  $\text{CH}_4$  partial pressure in the air (used as the headspace gas) of 405 and 1.85 ppm, respectively, and a mass balance for the headspace equilibration system. Full documentation of the calculations is available at the National Ecological Observatory Network's GitHub repository (<https://github.com/NEONScience/NEON-dissolved-gas>).

Water temperature, DO, and chl were measured using a YSI 6600 multiparameter sonde (Yellow Springs, Ohio, USA) with an optical DO sensor and barometric pressure was measured using a YSI MDS 650. The data sonde was calibrated prior to each field day, and the calibration was verified at the end of the day. Water samples for TP, TN, and TOC analysis were collected in new HDPE bottles triple rinsed with site water and stored on ice. Samples were stored at  $5^\circ\text{C}$  and analyzed within 24 h or frozen and analyzed within 28 days.

#### 2.5. Analytical

Methane,  $\text{CO}_2$ , and  $\text{N}_2$  were measured on a Bruker 450 gas chromatograph equipped with a flame ionization detector, methanizer, and thermal conductivity detector. Air, dissolved gas, and ebullition samples were analyzed in separate runs using a minimum of one 5-point standard curve bracketing the expected concentrations for each analyte. Standard curves were created using certified or primary standards and had a minimum  $r^2$  of 0.990, and standard checks were analyzed throughout analytical runs.

Automated colorimetry (Lachat Instruments QuickChem 8000 Flow Injection Autoanalyzer, Loveland, CO, USA) was used to measure TP following acid persulfate digestion (Bogren, 2001) and TN following alkaline persulfate digestion (Smith & Bogren, 2003). TOC was measured using high temperature oxidation and

NDIR detection (Shimadzu TOC-L/ASI-L). Quality control measures included standard curves, standard checks, laboratory blanks, and matrix spikes.

## 2.6. Data Analysis

### 2.6.1. Covariates

Potential predictor variables for modeling CO<sub>2</sub> and CH<sub>4</sub> emission rates include reservoir characteristics measured during the field campaign and those available in NHDPlusV2, lakeCat, and lakeMorpho, a group of related geo-spatial hydrologic data sets for the United States (Hill et al., 2018; Hollister & Stachelek, 2018; McKay et al., 2018).

Variables measured during the sampling campaign, hereafter “local” variables, include measures of water chemistry (TN, TP, TOC, chl, dissolved CO<sub>2</sub>, and dissolved CH<sub>4</sub>) and relative volumes of the hypoxic layer (oxygen saturation < 5%) and hypolimnion. We defined the hypolimnion as the water layer below the plane with the greatest temperature gradient. Lakes where the temperature gradient did not exceed 1 C m<sup>-1</sup> were considered unstratified.

NHDPlusV2, lakeCat, and lakeMorpho covariates, hereafter “national” variables, include reservoir area, perimeter, max depth, mean depth, proportion littoral, climate data, and 128 variables describing watershed characteristics (i.e., land use, size, and soil properties). We recalculated the estimates of basin shape (i.e., depth) in NHDPlusV2, which were modeled based on the surrounding terrain (Hollister et al., 2011), using-digitized bathymetric maps. We used the morphology descriptors included in the “national” variables to calculate additional morphology descriptors. Shoreline development factor (D; Kalff, 2002) was calculated as

$$D = \frac{L}{2(A\pi)^{0.5}}$$

where  $L$  is perimeter and  $A$  is area. Reservoir circularity ( $C$ ), lake area relative to that of a perfect circle with circumference equal to  $L$ , was calculated as

$$C = 4\pi AL^{-2}$$

Dynamic ratio (DR; Hakanson, 1982), an index related to the fraction of the lake bottom subject to erosion/resuspension from wind induced mixing, was calculated as

$$DR = \frac{A^{0.5}}{\bar{z}}$$

where  $\bar{z}$  is mean depth calculated as the ratio of reservoir volume and surface area. The lakeMorpho data set includes estimates of reservoir volume, but we recalculated volume using ArcGIS (ESRI, Redlands, CA, USA) and the digitized bathymetry. Depth ratio was calculated as the ratio of mean to maximum depth (Kalff, 2002) and the proportion of the lake <3 m deep, an index for littoral zone extent, was calculated using ArcGIS and the digitized bathymetry.

The list of potential predictor variables was reduced to those for which we hypothesized a relationship with CH<sub>4</sub> and/or CO<sub>2</sub> emissions. Correlation among predictor variables does not affect BRT prediction performance but can confound model interpretation (Fox et al., 2017; Freeman et al., 2016). We therefore omitted one variable from any pair with a Pearson correlation coefficient > 0.9. Variable pairs that were more weakly correlated but were likely to complicate model interpretation, were scrutinized, and in some cases, one variable in the correlated pair was dropped. For example, previous studies have shown that CH<sub>4</sub>-D is negatively related to lake size (Rasilo et al., 2015) and positively related to shoreline development factor (Bevelhimer et al., 2016); however, these two variables were inversely correlated in our data set ( $R = 0.11$ ), as has been reported in other studies (Winslow et al., 2014). This correlation could confound model interpretation; therefore, shoreline development factor was omitted. The final list of predictor variables in the model consisted of 8 local and 12 national variables (Table 1).

### 2.6.2. Boosted Regression Trees

We modeled reservoir GHG emission rates using boosted regression tree (BRT) models, a type of machine learning (ML) algorithm. Given a sufficiently large training data set, ML algorithms have been shown to have better prediction accuracy than general linear models (glms) (Elith et al., 2008) and are increasingly

**Table 1**  
Predictor Variables Used in Boosted Regression Trees to Model Methane and Carbon Dioxide Emission Rates

Variable	Units	Mean	Range
<i>Local Variables</i>			
chl	$\mu\text{g L}^{-1}$	17.2	1.5–61.4
TP	$\mu\text{g L}^{-1}$	84.3	7.9–772.7
TN	$\mu\text{g L}^{-1}$	1,202.9	231.4
TOC	$\text{mg L}^{-1}$	5.3	–3,463.0
<sup>a</sup> Dissolved CH <sub>4</sub>	$\mu\text{mol L}^{-1}$	3.58	2.5–15.4
<sup>a</sup> Dissolved CO <sub>2</sub>	$\mu\text{mol L}^{-1}$	121.4	0.43–18.55
Proportion Hypoxic	--	0.11	26.0–244.9
Proportion Hypolimnetic	--	0.22	0–0.69
<i>National Variables</i>			
Max Depth	m	13.3	0–0.73
Depth Ratio	--	0.39	2.7–35.1
Dynamic Ratio	--	0.57	0.16–1.13
Proportion <3 m Deep	--	0.42	0.12–1.80
<sup>b</sup> Reservoir Area	$\text{km}^2$	6.27	0.01–1.0
Relative Drainage Area	--	82.7	1.04–32.2
Percent Agriculture	%	43.5	5.7–385.9
Percent Agriculture on Slopes > 10%	%	34	0.1–83.9
Surface Soil Erodibility Factor	--	0.38	0–17.3
Soil Organic Matter	% by weight	0.97	0.31–0.43
Runoff	mm	405	0.31–6.20
30-Year Normal Mean Air Temperature	C°	10.6	325–520

<sup>a</sup>Units of  $\text{mol L}^{-1}$  were used in boosted regression tree models. <sup>b</sup>Units of  $\text{m}^2$  were used in boosted regression tree models.

used to model GHG emission rates in wetlands, lakes, and reservoirs (Chen et al., 2018; Mosher et al., 2015; Papale & Valentini, 2003).

Boosted regression trees consist of a collection of decision trees, where each tree is a statistical model that partitions the predictor space into regions that have the most homogenous values for a response variable (Breiman et al., 1984; Elith et al., 2008). Typical tree-based methods generate a single tree, whereas BRT generates many trees using modern boosting algorithms (Schapire, 2003) and combines them for prediction. This type of ensemble approach is based on the idea that individual trees often overfit the training data and result in noisy predictions. Averaging across many trees reduces the variance of the model and improves prediction accuracy.

We constructed separate BRT models for diffusive, ebullitive, and total CO<sub>2</sub> and CH<sub>4</sub> emission rates. Two types of models were constructed for each response variable; the first model type used only the “national” covariates while the second model type used both the “local” and “national” covariates. This allowed us to assess (1) how well emission rates can be modeled using variables available for all waterbodies in NHDPlusV2 and (2) how much prediction accuracy improves when “local” information is included in the model.

We constructed 50 BRT models for each response and covariate combination using the gbm package (Ridgeway, 2017) in R. To minimize overfitting, each model was trained using 90% of the observations collected during this field study and tested against the remaining 10%. Cross validation on the training data set was used to further minimize overfitting. To generate a training data set that reflected the full range of patterns across the 32 observations, the data were classified into five clusters, using *k*-means clustering, and the training data randomly selected from these five groups. A different training data set was generated for each BRT.

Each observation in the training data was weighted by the inverse of the variance of the reservoir-scale emission rate estimate. As described above (section 2.1), the variance was estimated from the GRTS survey design for each waterbody. This approach gave greater weight to well-constrained observations and less weight to more uncertain observations.

The optimal number of trees for each BRT was calculated as the number of trees beyond which model performance no longer improved. Only BRTs with an optimal number of trees >1,000 were accepted (Elith et al., 2008). Final BRT model performance was quantified as the mean square prediction error (MSE) calculated separately for the training data (in-sample or isMSE) and the 10% of the observations excluded from the training data (out of sample or osMSE). The collection of 50 BRTs for each response and covariate combination were ranked according to isMSE and osMSE. We defined the best model as the one with lowest sum of in and out of sample MSE rank, reflecting a balance between in and out of sample prediction error. Giving equal weight to in-sample and out-of-sample prediction error further minimized overfitting.

Standardized root-mean-square error (SRMSE) was calculated for all final models

$$\text{osSRMSE} = (\text{osMSE}^{0.5}) (\text{mean response}^{-1})$$

$$\text{isSRMSE} = (\text{isMSE}^{0.5}) (\text{mean response}^{-1})$$

where “mean response” is the mean of the observed response variable in the training data. SRMSE is a measure of relative error and is therefore useful for comparing model performance across different response variables.

We use partial dependence plots, created with the pdp library (Greenwell, 2017), to visualize relationships between response and predictor variables. Partial dependence plots provide a visualization of the relationship between the response and one predictor variable while accounting for the average effect of the other

predictors in the model. The relative influence of predictor variables was calculated based on the number of times a variable is selected for splitting, weighted by the squared improvement to the model following each split, and scaled so that the sum of all variables adds to 100 (Elith et al., 2008).

### 2.6.3. Upscaling

We used the BRT to predict total CH<sub>4</sub> emission rates for a subset of waterbodies contained in the waterbodies layer of the NHDPlusV2 database for the U.S. state of Ohio. The sample sites are distributed across the three main ecoregions in the state (Figure 1), span a broad range of land use conditions and reservoir morphometry, and are therefore representative of the environmental gradients most likely to affect emission rates. We adopted a state boundary to define our region of interest, rather than a more ecologically meaningful boundary, to facilitate comparison with emission sources in the FLIGHT database (<https://ghgdata.epa.gov/ghgp/main.do>) and anthropogenic GHG inventory (US Environmental Protection Agency, 2019b), both of which report emissions by state.

Reservoirs were identified from NHDPlusV2 Ohio waterbodies with FTYPE values of “LakePond” or “Reservoir” and surface area >8 Ha. Smaller waterbodies (e.g., ponds) are given separate treatment in the IPCC methodology (Lovelock et al., 2019) and are not addressed here. Because the FTYPE codes in NHDPlusV2 do not reliably discriminate reservoirs from natural lakes (Clow et al., 2015), we used the following additional criteria to identify reservoirs: (1) an FTYPE value of “reservoir” in NHDPlusV2, (2) GNIS name contained “reservoir,” (3) previous National Lakes Assessments (<https://www.epa.gov/national-aquatic-resource-surveys/nla>) site visits classified the waterbody as “man made,” or (4) were located in close proximity to a dam in the NID database (United States Army Corps of Engineers, 2013). Finally, the identified waterbodies were merged with the lakeCat and lakeMorpho databases to capture catchment and morphology descriptors.

To upscale to an annual estimate, we assumed (1) our measured rates were representative of April–October conditions (7 months) and (2) emission rates declined to a low and constant rate of 1 mg CH<sub>4</sub> m<sup>−2</sup> h<sup>−1</sup> from November to March (Beaulieu et al., 2014; <https://ameriflux.lbl.gov/sites/siteinfo/US-Act>; Beaulieu et al., 2018). We calculated 95% confidence intervals for the upscaled emission estimate by repeating the calculations 1,000 times where each calculation was based on a bootstrapped sample (with replacement) of the reservoirs in Ohio (Efron, 1979). This nonparametric manner of estimating uncertainty is well-accepted in the statistical literature and allows the modeler to simulate replication by subsampling the data set a large number of times.

## 3. Results

### 3.1. Basic Site Description

The survey design resulted in a collection of reservoirs spanning a broad range of morphological and chemical conditions. Sampled reservoirs ranged from 1 to 32 km<sup>2</sup> in surface area (median = 4.6 km<sup>2</sup>) with maximum depths ranging from 2.7 to 35 m (median = 11.0 m) (Table 1). Watershed land use across the 32 reservoirs was predominantly cultivated lands in the western portion of the study area transitioning into forested lands in the east and south (Figure 1). This broad range of watershed condition was reflected in the water chemistry with TP, TN, and chl ranging from 7.9 to 773, 231 to 3,463, and 1.5 to 61.4 μg L<sup>−1</sup> across the study sites, respectively, and exhibiting positive correlation with percent cultivated land in the watershed ( $R = 0.36, 0.78, \text{ and } 0.50$ , respectively). Twenty-four reservoirs were thermally stratified at the deepest sampling site and 22 reservoirs had hypoxic bottom waters.

### 3.2. Emission Rates

Dissolved CH<sub>4</sub> was supersaturated at all sites (Table 1; range 0.43–18.55 μmol L<sup>−1</sup>, median = 2.95 μmol L<sup>−1</sup>), indicating that all reservoirs were a source of CH<sub>4</sub> to the atmosphere. This was reflected in CH<sub>4</sub>-D which ranged from 0.03 to 21.99 mg CH<sub>4</sub> m<sup>−2</sup> h<sup>−1</sup> across the 491 individual measurements that met the modeling acceptance criteria (see section 2). When aggregated to the reservoir-scale, CH<sub>4</sub>-D ranged from 0.11 to 4.95 mg CH<sub>4</sub> m<sup>−2</sup> h<sup>−1</sup> (Figure 2; median = 1.26 mg CH<sub>4</sub> m<sup>−2</sup> h<sup>−1</sup>). Methane ebullition rates ranged from 0 to 155.4 mg CH<sub>4</sub> m<sup>−2</sup> h<sup>−1</sup> (Figure 2; median = 0.96 mg CH<sub>4</sub> m<sup>−2</sup> h<sup>−1</sup>) across 536 individual measurements and averaged 5.0 mg CH<sub>4</sub> m<sup>−2</sup> h<sup>−1</sup> at the reservoir scale (range: 0.1–22.8 mg CH<sub>4</sub> m<sup>−2</sup> h<sup>−1</sup>). Bubble CH<sub>4</sub> content ranged from 0.01 to 86.3% CH<sub>4</sub> (median = 57.4%,  $n = 336$ ) and was inversely related to bubble N<sub>2</sub>



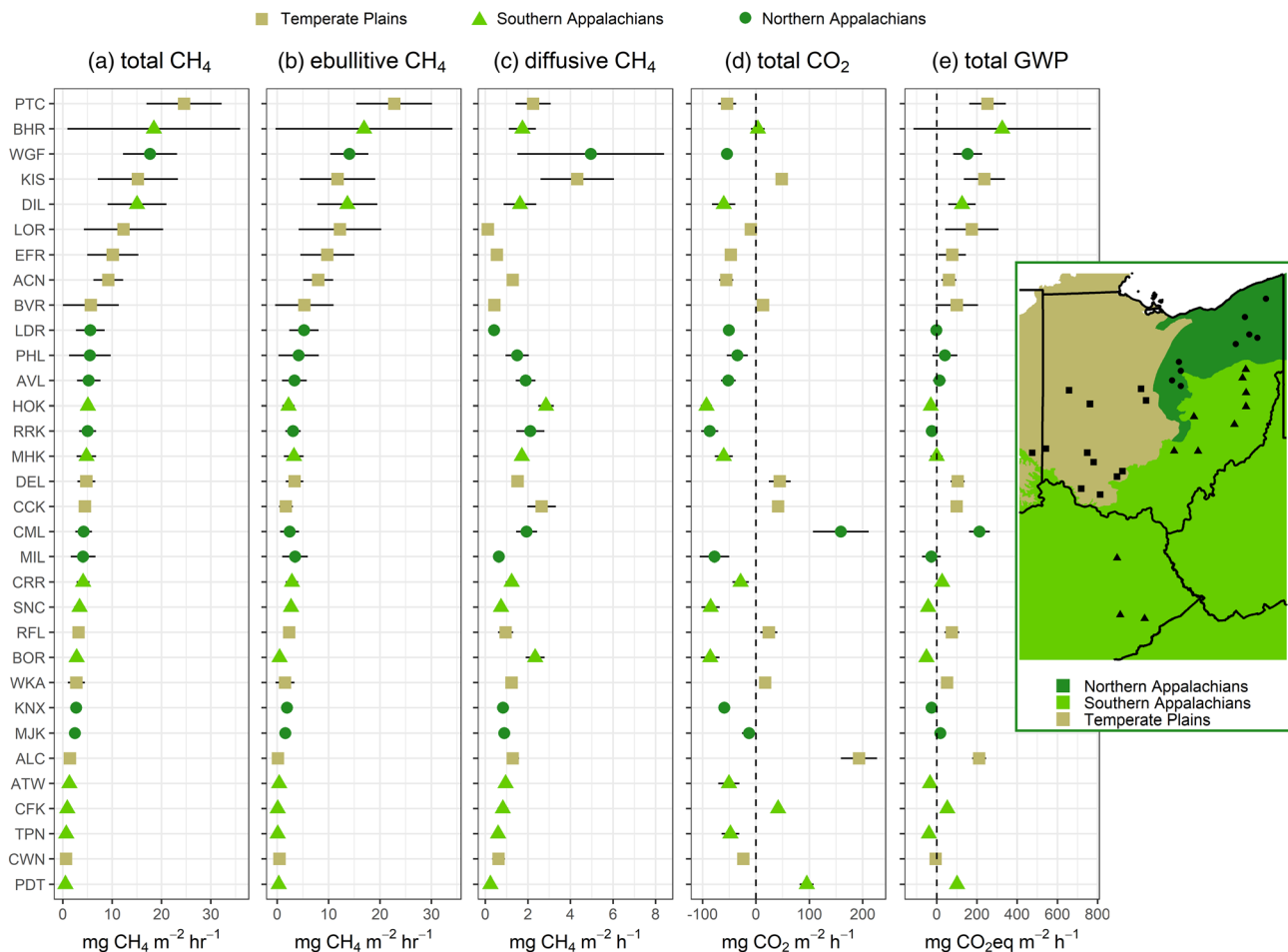


**Figure 2.** Reservoir scale mean emission rates and 95% confidence interval for (a) total CH<sub>4</sub> emissions, (b) ebullitive CH<sub>4</sub> emissions, (c) diffusive CH<sub>4</sub> emissions, (d) total CO<sub>2</sub> emissions, and (e) global warming potential (GWP). Vertical dashed line in panels (d) and (e) indicate emission rates of 0. Inset map shows location of study sites relative to the states of Ohio, Kentucky, Indiana, and the three major ecoregions in the study area.

content (Figure 3a). Total CH<sub>4</sub> emission rates (diffusive + ebullitive) ranged from 0.03 to 155.4 mg CH<sub>4</sub> m<sup>-2</sup> h<sup>-1</sup> across all point measurements and averaged 6.37 mg CH<sub>4</sub> m<sup>-2</sup> h<sup>-1</sup> when aggregated to the whole-reservoir scale (Figure 2; range: 0.51–24.57 mg CH<sub>4</sub> m<sup>-2</sup> h<sup>-1</sup>). Total CH<sub>4</sub> emission rates ranged from 5.1 to 12.3 mg CH<sub>4</sub> m<sup>-2</sup> h<sup>-1</sup> across the four surveys at Acton Lake (Table 2) with an overall mean ( $\pm 95\%$  CI) of  $9.2 \pm 3.0$ . The total CH<sub>4</sub> emission rate was greater in the tributary than open-water strata in 21 of the 27 reservoirs where a stratified survey design was used, although the difference was statistically significant in only 8. On average, ebullition composed 65% of total CH<sub>4</sub> emissions (range: 11–99%) with diffusive emissions accounting for the balance.

Dissolved CO<sub>2</sub> ranged from 26.0 to 244.9  $\mu\text{mol L}^{-1}$  (Table 1, median = 113.5  $\mu\text{mol L}^{-1}$ ), equivalent to 28–278% of the saturation value. Reservoir scale CO<sub>2</sub>-D ranged from –92.8 to 193.1 mg CO<sub>2</sub> m<sup>-2</sup> h<sup>-1</sup> (median = –41.0 mg CO<sub>2</sub> m<sup>-2</sup> h<sup>-1</sup>). Trapped bubbles contained minor amounts of CO<sub>2</sub> (range: 0.02–8.8%, median = 0.19%) and CO<sub>2</sub> ebullition constituted only 0.63% of total CO<sub>2</sub> emissions, on average. Reservoir-scale CO<sub>2</sub>-T ranged from –93 to 193 mg CO<sub>2</sub> m<sup>-2</sup> h<sup>-1</sup> (Figure 2, median = –40 mg CO<sub>2</sub> m<sup>-2</sup> h<sup>-1</sup>) and 21 reservoirs exhibited net CO<sub>2</sub> uptake during the measurement campaign (Figure 2d).

Although all 32 reservoirs were CH<sub>4</sub> sources during the survey, the GWP of these emissions was completely offset by CO<sub>2</sub> uptake in 11 reservoirs, yielding a net negative GWP for combined CH<sub>4</sub>/CO<sub>2</sub> emissions using the 100-year time horizon (Figure 2e). The remaining 21 reservoirs yielded a positive net GWP of CO<sub>2</sub>/CH<sub>4</sub> emissions, despite 10 of them functioning as CO<sub>2</sub> sinks. If the 20-year GWP was used to compare CH<sub>4</sub> to CO<sub>2</sub>, all reservoirs would have had larger and more positive combined GWP.

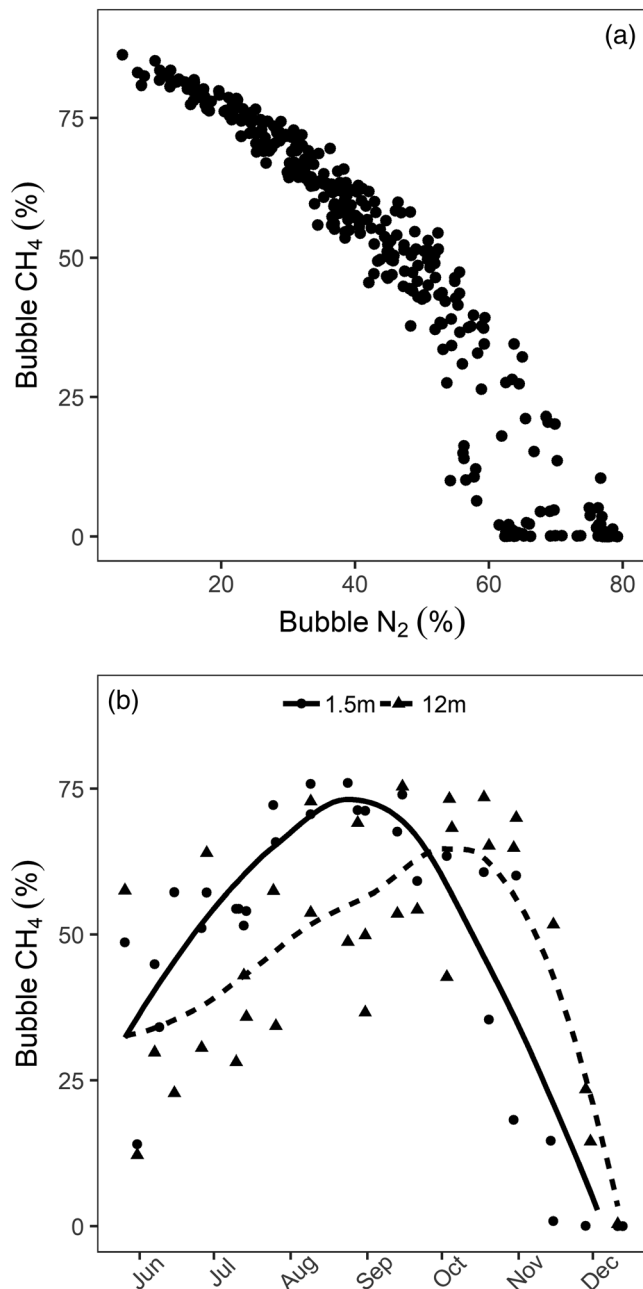


**Figure 3.** (a) CH<sub>4</sub> and N<sub>2</sub> content of bubbles collected during the 2016 survey. (b) Bubble CH<sub>4</sub> content during 2 years (2017–2018) of biweekly sampling at a deep (12 m) and shallow (1.5 m) site at Acton Lake. Solid and dashed lines represent LOESS smoothers.

**Table 2**  
Total Methane Emission Rates (Mean [95% C.I.]) Measured During Four Surveys Conducted at Acton Lake

Sample dates	CH <sub>4</sub> -T (mg m <sup>-2</sup> h <sup>-1</sup> )
2016-05-31	5.1 (3.6–6.6)
2017-07-10	8.2 (5.1–11.3)
2017-08-31	11.2 (7.5–14.9)
2017-10-04	12.3 (8.7–16.0)
Overall Mean	9.2 (6.2–12.2)

### 3.3. Boosted Regression Trees

Boosted regression trees for diffusive, ebullitive, and total CH<sub>4</sub> emission rates fit the data well with isSRMSE values ranging from 0.11 to 0.40 and  $R^2$  values for predicted versus observed (in-sample) ranging from 0.87 to 0.99 (Table 3 and Figure S1). Model predictions were less accurate at high emission rates, likely because these observations had larger confidence intervals (Figure 2) and were therefore given less weight in the model. As expected, model performance was somewhat greater when assessed against the training data than testing data. On average, osSRMSE values for the CH<sub>4</sub> models were 78% greater than isSRMSE values. Model performance was best for the total CH<sub>4</sub> emission rate, followed by ebullitive and diffusive emission rates. Combining local covariates (i.e., nutrient chemistry) with national covariates (i.e., watershed land use) improved CH<sub>4</sub> model performance when assessed against the training data but not when assessed against the testing data.

Indicators of watershed agricultural land use were important predictors in all CH<sub>4</sub> models and descriptors of reservoir morphology were important predictors in most CH<sub>4</sub> models (Table 4 and Figure 4). Reservoir area predicted diffusive CH<sub>4</sub> emissions and max depth predicted ebullitive and total CH<sub>4</sub> emissions. The BRT that included local covariates for CH<sub>4</sub>-D identified TOC, dissolved CH<sub>4</sub>, and TP as important predictors. Proportion hypolimnetic and dissolved CO<sub>2</sub> were important local predictors for CH<sub>4</sub>-E and CH<sub>4</sub>-T.

Prediction accuracy of the CO<sub>2</sub>-T BRT was worse than that of the CH<sub>4</sub> models (Table 3). The CO<sub>2</sub>-T model informed by only national covariates identified littoral extent and agricultural on steep slopes as important predictors. The addition of local covariates, particularly dissolved CO<sub>2</sub>, improved model performance.

### 3.4. Upscaling

We identified 280 reservoirs in Ohio greater than 8 Ha. These reservoirs have a cumulative surface area of 479 km<sup>2</sup> and emit 21.3 (13.3–30.8) Gg of CH<sub>4</sub> per year.

## 4. Discussion

### 4.1. CH<sub>4</sub> Emission Rates

CH<sub>4</sub>-T estimates for the individual reservoirs included in this study are reasonably well constrained and compare well to the literature. Total CH<sub>4</sub> emission rates measured in our diverse collection of 32 reservoirs spanned an order of magnitude (0.51–24.57 mg CH<sub>4</sub> m<sup>-2</sup> h<sup>-1</sup>), with higher rates occurring predominantly in the agricultural plains in the northwestern portion of the study region and lower rates in the Appalachian foothills of the eastern and southern portions of the study region (Figure 2). These emission rates are within the range reported for reservoirs worldwide (Deemer et al., 2016) and are comparable to values reported for other reservoirs in this region. In an investigation of six large, forested reservoirs in the southeastern United States, Bevelhimer et al. (2016) reported reservoir-scale CH<sub>4</sub>-T ranging from 0.04 to 1.07 mg CH<sub>4</sub> m<sup>-2</sup> h<sup>-1</sup>, similar to our values for forested reservoirs in the eastern and southern portions of our study (i.e., PDT and CFK). Beaulieu et al. (2018) monitored CH<sub>4</sub>-T at William H. Harsha Lake, an agricultural

**Table 3**

Standardized Root-Mean-Square Error (SRMSE) of Boosted Regression Tree Predictions Against Training and Testing Data for Diffusive, Ebullitive And Total CH<sub>4</sub> and CO<sub>2</sub> Emission Rates

Response variable	Covariates	Optimal trees	Training			Testing	
			isMSE	isSRMSE	R <sup>2</sup>	osMSE	osSRMSE
Diffusive CH <sub>4</sub>	national	12,803	0.38	0.40	0.87	0.41	0.42
	national + local	19,976	0.17	0.26	0.90	0.54	0.46
Ebullitive CH <sub>4</sub>	national	19,987	1.72	0.24	0.98	2.28	0.28
	national + local	16,760	0.52	0.13	0.99	3.42	0.33
Total CH <sub>4</sub>	national	19,984	0.91	0.15	0.99	0.46	0.11
	national + local	17,190	0.56	0.11	0.99	5.55	0.34
Total CO <sub>2</sub>	national	14,813	1,565	−4.29	0.73	734	−2.94
	national + local	8,935	730	−1.65	0.91	274	−1.01

*Note.* Coefficient of determination (R<sup>2</sup>) of model predictions is reported for testing data. The “national” covariates are predictor variables available from the National Hydrography Dataset (NHDPlusV2) and related data products. The “national + local” covariates include NHD variables and additional measurements made on-site during the field survey (i.e., nutrient chemistry).

reservoir in southwestern Ohio that was also included in this study (EFR), and reported an average CH<sub>4</sub>-T of 34.3 mg CH<sub>4</sub> m<sup>−2</sup> h<sup>−1</sup> between April and December 2015, which is similar to the highest rate observed during this study (mean ±95% CI: 24.6 ± 7.59 mg CH<sub>4</sub> m<sup>−2</sup> h<sup>−1</sup>), but higher than the current Harsha Lake measurement (mean ±95% CI: 10.1 ± 5.2 mg CH<sub>4</sub> m<sup>−2</sup> h<sup>−1</sup>), likely due to daily/seasonal variation in emission rates (section 4.2) and/or differences in measurement methods between sampling campaigns (Beaulieu et al., 2018). Although there are few published studies of CH<sub>4</sub> emission rates from reservoirs in this region of the United States, the available data suggest a pattern of increasing emission rates across an agricultural to forested land use gradient.

Because CH<sub>4</sub> is a relatively insoluble gas, it is often emitted in the form of bubbles that are released from the sediment and rise through the water column. Ebullition was an important emission mechanism in this study, comprising >50% of total CH<sub>4</sub> emissions in 75% of the 32 sampled reservoirs (Figure 2). This compares well to reports that ebullition contributes 65% of total CH<sub>4</sub> emissions from individual reservoirs (Deemer et al., 2016) and between 40% and 60% of total emissions from individual natural lakes (Bastviken et al., 2004). Comparison of CH<sub>4</sub>-E among lakes and studies can be complicated, however, by differences in bubble composition. The CH<sub>4</sub> content of bubbles collected in this study ranged from 0.01 to 86.3% CH<sub>4</sub> (median = 57.4%), similar to the range previously reported for lakes (Walter et al., 2008) and reservoirs (Beaulieu et al., 2018; Harrison et al., 2017; Koschorreck et al., 2017). Bubble CH<sub>4</sub> content was inversely related to N<sub>2</sub> content (Figure 3a), a pattern which has also been observed in lakes and wetlands (Chanton et al., 1989; Nakagawa et al., 2002; Walter et al., 2008) and is attributed to N<sub>2</sub> stripping. N<sub>2</sub> stripping occurs when ebullition removes N<sub>2</sub> from porewaters more quickly than it is replenished via diffusion from the overlying water column, thereby depleting sediment N<sub>2</sub> content and enriching the CH<sub>4</sub> content of rising bubbles (Chanton et al., 1989). Stripping likely contributed to the increasing bubble CH<sub>4</sub> content from June through October observed at Acton reservoir (ACT; Figure 3b). Falling bubble CH<sub>4</sub> content in November and December likely reflects decreasing volumetric ebullition rates as the water column cooled, allowing diffusion to replenish porewater N<sub>2</sub>. Patterns in porewater N<sub>2</sub> stripping, in combination with temporal changes in temperature, organic matter availability, and other factors, can lead to complex spatial and temporal patterns in CH<sub>4</sub> ebullition.

#### 4.2. Survey and Measurement Approach

Although it is becoming increasingly evident that ebullition is an important CH<sub>4</sub> emission mechanism in lentic waters, it remains challenging to quantify due to strong spatial and temporal variability. In this study, we characterized spatial variability within the framework of a GRTS design (see section 2.1). Features of the GRTS design that make it particularly well suited for estimating CH<sub>4</sub>-E and CH<sub>4</sub>-T include (1) a spatially balanced distribution of sampling sites (Olsen et al., 2012), thereby better representing the full range of environmental conditions present within a waterbody as compared to random sampling, and (2) the ability to utilize spatial autocorrelation to better constrain variance estimates. In this study, variance estimates were reduced by 23% when spatial autocorrelation was incorporated into the estimate, indicating strong spatial

**Table 4**

*List of Covariates Leading to an Average of at Least a 5% Reduction in Mean Square Error When Excluded From the Model*

Response variable	Covariates	Variable	Relative influence
CH <sub>4</sub> -D	National and local covariates	TOC	15.7
		ag on slope > 10%	14.6
		dissolved CH <sub>4</sub>	14.6
		reservoir area	12.8
		TP	12.4
		proportion <3 m deep	5.9
		soil organic matter	5.1
CH <sub>4</sub> -D	National covariates	reservoir area	23.0
		ag on slope > 10%	14.3
		soil organic matter	10.1
		percent ag	9.4
		dynamic ratio	8.4
		relative drainage area	6.6
		depth ratio	5.9
CH <sub>4</sub> -E	National and local covariates	proportion <3 m deep	5.6
		relative drainage area	25.2
		proportion hypolimnetic	17.4
		percent ag	13.1
		dissolved CO <sub>2</sub>	9.3
		max depth	9.1
		proportion hypoxic	6.2
CH <sub>4</sub> -E	National covariates	relative drainage area	21.4
		percent ag	15.3
		dynamic ratio	10.3
		soil erodibility factor	9.4
		ag on slope > 10%	7.7
		proportion <3 m deep	7.4
		depth ratio	7.1
CH <sub>4</sub> -T	National and local covariates	max depth	6.6
		mean air temperature	6.3
		soil organic matter	29.7
		depth ratio	11.8
		relative drainage area	10.1
		percent ag	8.0
		dissolved CO <sub>2</sub>	7.3
CH <sub>4</sub> -T	National covariates	ag on slope > 10%	6.9
		proportion hypolimnetic	5.7
		relative drainage area	21.6
		depth ratio	20.0
		max depth	16.6
		percent ag	11.6
		proportion < 3 m deep	7.0
CO <sub>2</sub> -T	National and local covariates	runoff	5.1
		dissolved CO <sub>2</sub>	47.4
		ag on slope > 10%	14.5
		proportion hypoxic	6.9
		percent ag	6.1
CO <sub>2</sub> -T	National covariates	TP	5.8
		depth ratio	23.8
		proportion < 3 m deep	19.2
		runoff	15.8
		relative drainage area	9.2
		ag on slope > 10%	7.8
		reservoir area	6.9
		soil erodibility factor	5.0

*Note.* These represent the most important variables in each boosted regression trees are listed in order of decreasing importance for each model.



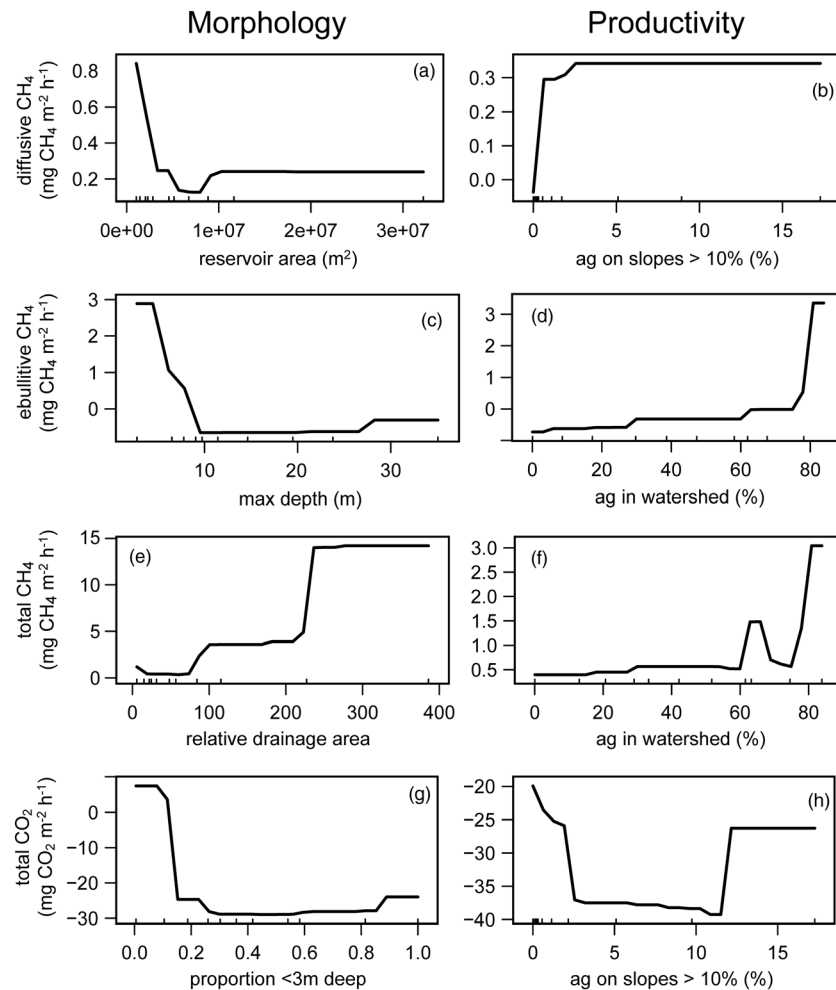


**Figure 4.** Partial dependence plots for boosted regression trees using only national covariates for (a and b) diffusive  $\text{CH}_4$  emission rates, (c and d) ebullitive  $\text{CH}_4$  emission rates, (e and f) total  $\text{CH}_4$  emission rates, and (g and h) total  $\text{CO}_2$  emission rates. Vertical ticks along x axis represent observations included in the training data.

autocorrelation in  $\text{CH}_4$ -T, as has been reported elsewhere (Beaulieu et al., 2016; Hilgert et al., 2019). The median 95% confidence intervals for  $\text{CH}_4$ -T and  $\text{CO}_2$ -T were 72.3% and 58.2% of the mean emission rate, respectively. Given that the observed  $\text{CH}_4$  emission rates spanned 2 orders of magnitude in this study, an uncertainty estimate equivalent to  $\sim 70\%$  of the mean is acceptable for the purposes of training a model for predicting emissions at unsampled locations. Furthermore, our modeling approach used the uncertainty estimate to give more weight to well constrained estimates, thereby ensuring that model results were not driven by highly uncertain observations. We suggest that studies of lentic  $\text{CH}_4$  and  $\text{CO}_2$  emission rates be based on robust survey designs that form the basis for well-defined variance estimates.

Sampling tributary-associated areas at a higher density than open-water areas allowed for a better constrained and more accurate population estimate than if the entire waterbody had been sampled at a uniform density. Other studies have attributed tributary associated  $\text{CH}_4$  hot spots to higher temperatures at the sediment-water interface, high sediment deposition rates, and sustained nutrient inputs from inflowing rivers which support phytoplankton, a source of particularly labile carbon for methanogens (De Mello et al., 2018; DelSontro et al., 2011; Grinham et al., 2011; Hilgert et al., 2019; Musenze et al., 2014; Sturm et al., 2014). Low water depths in tributary areas minimizes the dissolution of bubbles during vertical transport through the water column, further enhancing  $\text{CH}_4$  emissions (McGinnis et al., 2006). Our finding that tributaries supported higher  $\text{CH}_4$ -T than open waters in 21 of the 27 reservoirs where stratification was employed (although the difference was only statistically significant in 8) further highlights the importance of including tributary areas in reservoir-scale emission estimates.

Methane emission rates can exhibit temporal variation at time-scales ranging from hourly to yearly (Harrison et al., 2017; Maher et al., 2019; Natchimuthu et al., 2016). Our survey was designed to represent a snapshot of conditions during the growing season. Ebullition, the most important emission mechanism in most of the sampled reservoirs, was measured throughout ~19 h (median = 19.4 h) funnel deployments, encompassing roughly equal hours of daylight and dark. Our ebullition rate estimates should therefore integrate across diurnal patterns and reflect emission rates similar to 24 h daily integrated values. Diffusive emissions were measured during a short 5-min window of daylight, however, and could be biased if a diurnal pattern were present. While several studies have documented diurnal patterns in CH<sub>4</sub>-E (Deshmukh et al., 2014; Maher et al., 2019), the literature on diurnal patterns in CH<sub>4</sub>-D is somewhat mixed. For example, Carey et al. (2017) failed to find a consistent diurnal pattern in CH<sub>4</sub>-D in a productive U.S. reservoir. Natchimuthu et al. (2014) reported higher dissolved CH<sub>4</sub> concentrations during daylight hours in a small pond (average depth = 1.2 m), but it is not clear how patterns from a shallow pond would translate to patterns in our much larger reservoirs. Recent eddy covariance studies have shown evidence of diurnal patterns in CH<sub>4</sub> emission rates, but the results are mixed and it is difficult to distinguish ebullition and diffusion using this method (Erkkila et al., 2018; Podgrajsek et al., 2014). Given the conflicting and sparse literature data, it is difficult to know whether the short-term CH<sub>4</sub>-D measurements in this study are biased. Bias in CH<sub>4</sub>-D would not greatly affect the total emission rate estimate when ebullition was the dominant emission mechanism (Figure 2), as was the case in 75% of the sampled reservoirs, but would be a concern where CH<sub>4</sub>-D and CH<sub>4</sub>-E were similar.

The four surveys conducted at Acton Lake indicate that CH<sub>4</sub>-T can vary by up to a factor of 2.4 within the warm weather months (Table 2; range: 5.1–12.3 mg CH<sub>4</sub> m<sup>-2</sup> h<sup>-1</sup>). This variation could be caused by numerous factors including changes in hydrostatic pressure, which can trigger the release of bubbles stored in sediments (Harrison et al., 2017; Varadharajan & Hemond, 2012), availability of algal derived carbon (West et al., 2016), or extent of porewater N<sub>2</sub> stripping (section 4.1). While the temporal variability observed at Acton Lake was substantial, it was less than the variation observed across the 32 study sites (Figure 2; range: 0.51–24.57 mg CH<sub>4</sub> m<sup>-2</sup> h<sup>-1</sup>) or within Acton Lake during any of the four surveys (within lake CH<sub>4</sub>-T maximum exceeded minimum by a factor of 43, on average, data not shown), suggesting that spatial variability (both intra and inter reservoir) exceeds temporal variability. Nevertheless, temporal variability may introduce uncertainty and bias into model predictions. Sampling on randomly selected days, as was done in this study, is likely to miss episodic emission events, which appear to be responsible for most day to day variability in CH<sub>4</sub>-T (Varadharajan & Hemond, 2012), resulting in emission rate estimates that are biased low (Wik et al., 2016). Quantifying model uncertainty resulting from temporal variability is challenging, but emerging continuous monitoring approaches may allow for this in future studies (Jammet et al., 2017).

### 4.3. CO<sub>2</sub> Emission Rates

Ebullitive CO<sub>2</sub> emissions were negligible compared to diffusive emissions in most reservoirs. This pattern is expected because CO<sub>2</sub> is a relatively soluble gas with most produced CO<sub>2</sub> dissolving into the water column or pore waters, rather than accumulating in bubbles. Our findings are consistent with reports that CO<sub>2</sub>-E is less than 0.05% that of CO<sub>2</sub>-D in large reservoirs in the Southeastern United States and Brazil (Bergier et al., 2011; Bevelhimer et al., 2016; Kemenes et al., 2011), suggesting this pattern is common across a broad range of lentic ecosystems.

Reservoir-scale CO<sub>2</sub> emission rates were highly variable across the 32 reservoirs (−93–193 mg CO<sub>2</sub> m<sup>-2</sup> h<sup>-1</sup>), spanning nearly the entire range of reservoir CO<sub>2</sub> emission rates found in the published literature (−54.4–403 mg CO<sub>2</sub> m<sup>-2</sup> h<sup>-1</sup>; Deemer et al., 2016), reflecting the broad range of watershed and reservoir conditions in this study. Sixty five percent of the reservoirs functioned as CO<sub>2</sub> sinks during the sampling period, which contradicts findings from several global-scale and regional-scale studies. In a study of 1,835 lakes with a worldwide distribution, Cole et al. (1994) reported that only 13% were CO<sub>2</sub> sinks. Similarly, Deemer et al. (2016) found that only 16% of published studies report net CO<sub>2</sub> uptake in reservoirs and studies in boreal regions routinely report net CO<sub>2</sub> efflux (Sobek et al., 2003). Reports of CO<sub>2</sub> emission rates for U.S. lakes and reservoirs are more mixed, however. A national-scale survey of dissolved CO<sub>2</sub> found 35% of sampled U.S. waterbodies ( $n = 1,080$ ) to be CO<sub>2</sub> sinks with no coherent spatial pattern

(Lapierre et al., 2017), whereas regional studies suggest strong geographic variation. For example, measurements in the southeastern United States indicate net CO<sub>2</sub> evasion from >85% of sampled lakes and reservoirs ( $n = 954$ ) (Bevelhimer et al., 2016; Lazzarino et al., 2009), whereas surveys of lakes and reservoirs in the western and midwestern United States indicate a predominance of CO<sub>2</sub> uptake (Balmer & Downing, 2011; Soumis et al., 2004) during the summer months, particularly in systems draining agricultural watersheds. These contrasting results for U.S. waterbodies highlight the difficulty in predicting lentic CO<sub>2</sub> emission rates. This is also reflected in the poor prediction accuracy of the CO<sub>2</sub>-T BRT model developed in this work, relative to that of the CH<sub>4</sub>-T BRT. One possible explanation for this is that the controls on CO<sub>2</sub> emissions may vary across the major U.S. ecoregions. For example, Lapierre et al. (2017) found geographically varying driver-response relationship for dissolved CO<sub>2</sub> in U.S. waterbodies reflecting major landscape gradients across the country. The 32 reservoirs included in our study span three major ecoregions (Figure 1), roughly corresponding to regions identified by Lapierre et al. (2017) to have different dissolved CO<sub>2</sub> ~ driver relationships, suggesting that spatially explicit modeling approaches may improve prediction accuracy for lentic CO<sub>2</sub> emission rates.

Like many other studies of air-water CO<sub>2</sub> exchange in lentic ecosystems, we measured diffusive CO<sub>2</sub> emission rates during daylight hours. While these short-term measures of CO<sub>2</sub>-D have been used to inform global CO<sub>2</sub> budgets for lentic systems (Cole et al., 2007; DelSontro et al., 2018), they may not reflect a daily integrated rate. Diurnal changes in the relative rates of CO<sub>2</sub> uptake (photosynthesis) and production (respiration) can be pronounced, particularly in productive waterbodies, leading to higher emission rates during hours of darkness. This pattern has been reported for a wide range of lentic ecosystems including lakes in northern Europe, Canada, Brazil, and China (Du et al., 2018; Erkkila et al., 2018; Natchimuthu et al., 2014; Reis & Barbosa, 2014; Spafford & Risk, 2018; Vesala et al., 2006). Perhaps more relevant to the current study are reports from a eutrophic lake and reservoir in the southcentral United States (Liu et al., 2016; Xu et al., 2019). During the summer months, both systems alternated between a CO<sub>2</sub> source at night and sink during the day. Although we are unaware of diurnal CO<sub>2</sub> flux studies in our study region, the literature suggests that such patterns likely exist, and our measurements likely overestimate the daily CO<sub>2</sub> uptake or underestimate the daily CO<sub>2</sub> efflux.

#### 4.4. GWP of CO<sub>2</sub> and CH<sub>4</sub> Emissions

Although all 32 reservoirs were a source of CH<sub>4</sub> to the atmosphere, 11 reservoirs had a negative combined CO<sub>2</sub>/CH<sub>4</sub> GWP on a 100-year time horizon due to strong CO<sub>2</sub> uptake. This pattern has also been reported for small lakes in agricultural regions of the United States, causing speculation that high-nutrient lakes may be net atmospheric CO<sub>2</sub> sinks (Balmer & Downing, 2011) due to high rates of primary production. While many of the reservoirs in our study were net CO<sub>2</sub> sinks during daylight hours when CO<sub>2</sub>-D was measured, it is possible that daytime uptake was offset by nighttime emissions. It is also likely that CO<sub>2</sub> emissions exhibit strong seasonal patterns in these temperate-zone dimictic reservoirs. For example, a study of 15 reservoirs in the Glacial Till Plains of the United States found that all systems absorbed atmospheric CO<sub>2</sub> during the summer months but emitted CO<sub>2</sub> during the remainder of the year and were net CO<sub>2</sub> sources at the annual scale (Jones et al., 2016). A similar seasonal pattern was previously noted for Acton Lake, an agricultural reservoir included in this study, and Burr Oak, a forested reservoir located nearby our study sites (Knoll et al., 2013). Therefore, diel and seasonal measurements are required to accurately determine the CO<sub>2</sub> source/sink status of temperate zone reservoirs.

Although 21 of 32 reservoirs were CO<sub>2</sub> sinks during the measurement period, all were sources of CH<sub>4</sub> and the net GWP of CO<sub>2</sub>/CH<sub>4</sub> emissions was positive in 21 of the 32 sampled reservoirs for a 100-year time horizon, indicating that these systems contribute to the radiative forcing of the atmosphere. The GWP of CO<sub>2</sub> emissions exceeded that of CH<sub>4</sub> in only four reservoirs, in contrast with reports from six large reservoirs in the Southeastern United States where the GWP of CO<sub>2</sub> emissions exceeded that of CH<sub>4</sub>, suggesting there may be important regional variation in the relative importance of these GHGs. On national and global scales, however, the GWP of CH<sub>4</sub> emissions from lakes and reservoirs far outweighs that of CO<sub>2</sub> (Deemer et al., 2016; DelSontro et al., 2018; Li & Bush, 2015). Understanding the relative importance of these two gases in total reservoir GWP is important when considering mitigation strategies. For example, since CH<sub>4</sub> emissions are predominantly driven by ebullition, management actions that minimize the release of

CH<sub>4</sub> rich bubbles from sediments, such as avoiding water-level drawdowns during the summer months, may mitigate CH<sub>4</sub> emissions (Beaulieu et al., 2018; Harrison et al., 2017), but have little effect on CO<sub>2</sub> emissions. Reductions in the emission of both gases should follow management actions that reduce nutrient loading to surface waters, however (Beaulieu et al., 2019; Deemer et al., 2016). Policy makers should also use the appropriate GWP horizon to weigh the relative merits of CH<sub>4</sub> and CO<sub>2</sub> emission reductions in meeting mitigation goals.

#### 4.5. Model Performance

Fifty BRTs were developed for each response variable (e.g., CH<sub>4</sub>-T and CH<sub>4</sub>-D) and collection of covariates (e.g., national and national + local). Each BRT was trained and tested with unique subsets of the data and the accuracy of each model was quantified as the MSE of the predicted versus observed emission rates. We defined the best model as the BRT that had the lowest combined in-sample and out-of-sample MSE values, reflecting a balance between in-sample prediction accuracy and overfitting. MSE values for the best models were relatively low, even when tested against the proportion of the data not used for training the model (e.g., out-of-sample data) (Table 3). For example, the out-of-sample standardized root-mean-square error (osSRMSE), a measure of prediction error normalized to the mean response, ranged from 11% to 34% for CH<sub>4</sub>-T, depending on which covariates were included in the model. Considering CH<sub>4</sub>-T values spanned 2 orders of magnitude across the study and the well-established difficulty of predicting CH<sub>4</sub>-T, this prediction error is quite low.

Other regional scale studies have been largely unable to identify relationships between CH<sub>4</sub>-T and environmental drivers (Bevelhimer et al., 2016; Rinta et al., 2016), possibly because those studies used general linear modeling approaches, whereas the BRTs used in this work are better at accounting for nonlinear and interactive dynamics (Elith et al., 2008). Of course, the success of any modeling approach will be partly a function of the quality of the data being modeled. A strength of the current work is that the site selection criteria (e.g., broad land use and morphology gradient) resulted in a broad range of environmental conditions while the survey design (e.g., GRTS design per waterbody) enabled accurate emission estimates. Together, these features likely enabled the pattern detection reflected in the BRT results.

Since BRTs do not have native methods for estimating model uncertainty, unlike generalized linear models, we used an empirical bootstrap (Efron, 1979) to estimate the 95% confidence interval (C.I.) of the upscaled emission estimates for Ohio reservoirs. The bootstrap 95% C.I. was equivalent to 82% of the mean emission estimate, which is greater than uncertainty levels typically reported for U.S. anthropogenic CH<sub>4</sub> sources. For example, uncertainty in the magnitude of CH<sub>4</sub> emissions from enteric fermentation and landfills, the two largest anthropogenic CH<sub>4</sub> sources in the United States, is equivalent to 29% and 55% of the mean, respectively (U.S. Environmental Protection Agency, 2019b). Uncertainty in the estimated magnitude of reservoir CH<sub>4</sub> emissions could be reduced through (1) improved identification of reservoirs in the landscape and (2) greater data availability for training predictive models.

#### 4.6. Reservoir Morphology and CH<sub>4</sub>/CO<sub>2</sub> Emissions

The BRTs identified descriptors of reservoir morphology as important predictors of CH<sub>4</sub> emission rates, with indicators of reservoir size being particularly important. For example, the models predict a negative relationship between CH<sub>4</sub>-D and reservoir surface area (Figures 4a and S2e), as has been previously reported for boreal lakes (Rasilo et al., 2015). Small lakes and reservoirs have several characteristics that may promote CH<sub>4</sub>-D including extensive littoral habitat. Methane released from littoral sediments has a short residence time in the overlying shallow water column, thereby escaping oxidation that converts a large fraction of dissolved CH<sub>4</sub> to CO<sub>2</sub> in deeper waters. This phenomenon, termed the “epilimnetic shortcut,” has been demonstrated in several boreal lakes (Bastviken et al., 2008). While we did not measure CH<sub>4</sub> oxidation in this study, the BRTs predicted a positive relationship between littoral extent and rates of all three CH<sub>4</sub> emission mechanisms (i.e., diffusion, ebullition, and total), further suggesting that littoral areas are particularly important sites for CH<sub>4</sub> emissions (Figures S2g, S3h, S5f, and S7e).

Maximum reservoir depth was identified as an important predictor of reservoir-scale CH<sub>4</sub>-E, with rates falling rapidly from shallow systems to a max depth of 5–10 m, beyond which ebullition rates are predicted to remain low (Figures 4c, S4e, and S5h). This pattern is also evident at the scale of individual point



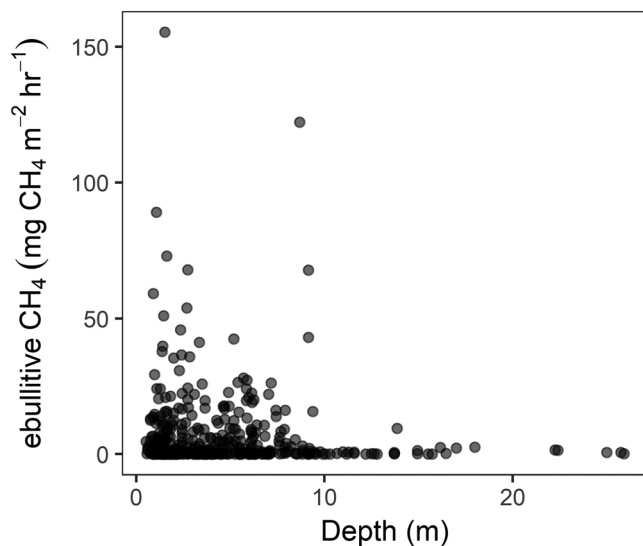


**Figure 5.** Ebullitive  $\text{CH}_4$  emission rate versus water depth for 536 point measurements across the 32 reservoirs in this study. Symbol shading reflects the number of observations at any  $x, y$  coordinate. Dark and light shadings reflect a high and low density of observations, respectively.

measurements where ebullition was uncommon beyond depths of  $\sim 10$  m (Figure 5). Ebullition–depth thresholds in the 5–10 m range have also been reported for lakes (West et al., 2016), suggesting this is a widespread pattern. The inverse relationship between ebullition rates and water depth is consistent with the well-established understanding that the total dissolved gas pressure required for bubble formation is proportional to the hydrostatic pressure at the sediment–water interface (Boudreau et al., 2005; Mattson & Likens, 1990; Scandella et al., 2011); therefore, more biogenic gas production is required to support bubble formation in deep versus shallow waters. While this pattern has been previously demonstrated for lakes, our work illustrates that the conceptual model also holds for reservoirs.

The BRTs identified a positive relationship between relative drainage area (RDA) and total  $\text{CH}_4$  emission rates (Figure 4e). Relative drainage area is the ratio of watershed-to-reservoir surface area and is positively correlated with carbon, nitrogen, and phosphorus burial rates in our study area (Knoll et al., 2014). We suggest that RDA serves as a proxy for sedimentation rates which can stimulate  $\text{CH}_4$  production by supplying reactive organic matter to deep, anoxic sediment, thereby fueling methanogenesis (Sobek et al., 2012). Several studies have shown correlations between sedimentation rates and  $\text{CH}_4$  emission rates in reservoirs, including Harsha Lake, a reservoir sampled in this study (Berberich et al., 2019; De Mello et al., 2018; Maeck et al., 2013). While sedimentation rates may be important drivers of  $\text{CH}_4$  production, the composition of watershed derived particulate matter may also play a role. The BRT also identified a positive relationship between the organic matter content of watershed soils and  $\text{CH}_4\text{-T}$  (Figure S6a), suggesting that organic rich material eroded from the watershed stimulates methanogenesis more effectively than inorganic materials.

The BRTs also identified relationships between  $\text{CO}_2\text{-T}$  and measures of reservoir morphology. The BRT predicts greatest  $\text{CO}_2$  uptake (i.e., a more negative  $\text{CO}_2$  emission rate) in small reservoirs with extensive littoral zone habitat (Figures 4g and S9f). This pattern contradicts a recent literature review indicating that  $\text{CO}_2$  emission rates increase (i.e., become more positive) with decreasing lake size (DelSontro et al., 2018). A possible explanation for this contradiction is that TP was negatively correlated with reservoir size in this study (pearson correlation coefficient =  $-0.15$ ); therefore, smaller reservoirs may have had greater nutrient availability and consequently higher rates of primary productivity. This explanation is consistent with the BRT model based on local + national covariates which predicts rapidly increasing  $\text{CO}_2$  uptake (i.e., more negative  $\text{CO}_2$  emission rates) as a function of TP concentration (Figure S8e). Another possibility is that littoral zone macrophytes, which can reach nuisance levels in these reservoirs (Davic et al., 1997), are a direct sink for dissolved  $\text{CO}_2$  (Madsen & Sandjensen, 1991).

#### 4.7. Primary Production and $\text{CH}_4/\text{CO}_2$ Emissions

Several studies have shown that lentic  $\text{CH}_4$  emission rates are correlated with system productivity, presumably because autochthony promotes hypolimnion anoxia and provides a source of labile carbon to methanogens (DelSontro et al., 2016, 2018; West et al., 2016). Our list of covariates included several indices of productivity, including estimates of watershed land use, a proxy for nutrient loading, and in-lake measures of chl and nutrient concentrations. Surprisingly, chl did not emerge as an important predictor variable in any of the BRT models, possibly because water column chl can vary greatly on hourly and daily time scales (Rusak et al., 2018), whereas methanogens are more tightly linked to sediment conditions which reflect productivity over longer time scales. The  $\text{CH}_4\text{-D}$  BRT showed mixed patterns in relation to productivity indices. The model predicted increasing  $\text{CH}_4\text{-D}$  with increasing agriculture on steep slopes (Figure 4b) but an inverse relationship with TP and watershed agricultural activity (Figures S2f and S3e). Patterns in the  $\text{CH}_4\text{-T}$  and  $\text{CH}_4\text{-E}$  BRT models were more intuitive, however, and demonstrate increasing emissions as a function of agricultural activity in the watershed (Figures 3d, 3f, S4c, S5b, S5e, S6d, and S6f). These patterns suggest that ebullitive and total  $\text{CH}_4$  emissions are more closely tied to watershed condition than are diffusive emission

rates, possibly because differential rates of CH<sub>4</sub> oxidation can obscure patterns between CH<sub>4</sub>-D and rates of methanogenesis, whereas ebullition is largely unaffected by CH<sub>4</sub> oxidation (West et al., 2016).

The relationships between CO<sub>2</sub>-T and indices of aquatic productivity were somewhat mixed. Both BRTs (i.e., national covariates only and national + local covariates) identified a general trend of increased CO<sub>2</sub> uptake (CO<sub>2</sub>-T became more negative) with increasing agriculture on steep slopes, though this relationship is somewhat obscured by one observation with widespread agriculture in the watershed, but relatively low CO<sub>2</sub> uptake (Figure 4h) in the national covariate model. The BRT utilizing local covariates also identified increasing CO<sub>2</sub> uptake with increasing TP (Figure S8e), another productivity proxy. Together, these patterns suggest that external nutrient loading, derived partly from watershed agricultural practices, stimulate aquatic primary productivity and CO<sub>2</sub> uptake, consistent with reports from other agricultural regions of the country (Balmer & Downing, 2011). These intuitive patterns are somewhat confounded, however, by a predicted decrease in CO<sub>2</sub> uptake (i.e., more positive CO<sub>2</sub>-T) with increasing agricultural in the watershed (Figure S8d), suggesting CO<sub>2</sub>-T responds differently to agricultural on steep versus gentle slopes, though we are unable to explain why this may be.

#### **4.8. Local Versus National Predictor**

We ran one set of BRTs informed with only those covariates available for all U.S. waterbodies included in NHDPlusV2 geodatabase and a second set of BRTs which also included “local” covariates measured during the field survey, including measures of water chemistry and algal abundance. We expected prediction accuracy to improve when local covariates were added to the model, and for CH<sub>4</sub>, this was the case when prediction accuracy was assessed against the training data, but not when assessed against the testing data (Table 3). Furthermore, prediction accuracy was quite good for all CH<sub>4</sub> models, regardless of whether local covariates were included, suggesting that CH<sub>4</sub> emission rates can be predicted for U.S. reservoirs using the existing NHDPlusV2 and derivative geodatabases, without the need for additional resource intensive fieldwork.

Unlike the CH<sub>4</sub> models, prediction accuracy for the CO<sub>2</sub>-T BRT model substantially improved when local covariates were included, due largely to the predictive power of dissolved CO<sub>2</sub> concentration. The BRT predicts a positive relationship between CO<sub>2</sub>-T and dissolved CO<sub>2</sub> (Figure S8a), which is consistent with well-established diffusive gas-exchange theory (MacIntyre et al., 1995). This phenomenon is also reflected in the CH<sub>4</sub>-D BRT which identified a positive relationship between dissolved CH<sub>4</sub> concentration and CH<sub>4</sub>-D (Figure S2c), as has been previously reported for lakes in the USA and Europe (Rinta et al., 2016). The model identified a negative relationship between CH<sub>4</sub>-D and TOC (Figure S2a), which may reflect an indirect relationship between TOC and CH<sub>4</sub> oxidation. Methanotrophs are inhibited by high light availability (Thottathil et al., 2018). Reduced light under high TOC conditions may therefore release methanotrophs from light inhibition, resulting in higher methanotrophic activity, lower dissolved CH<sub>4</sub> concentrations, and lower CH<sub>4</sub>-D.

#### **4.9. Limitations of Modeling Approach**

Many of the response–driver relationships captured by the BRTs are consistent with established theory and previously reported results, suggesting that the models are being driven, at least in part, by fundamental ecological processes, rather than statistical artifacts such as overfitting. Like all statistical models and ML algorithms, however, BRTs may overfit training data, particularly with smaller data sets. We implemented several procedures to minimize this risk including the use of different subsets of the data to train 50 BRTs for each response–covariate combination, cross validation to minimize overfitting within each training data set, a criterion specifying the minimum number of trees in an “acceptable” model, and a model selection criterion that gave equal weight to in-sample and out-of-sample performance. While these precautions minimize overfitting, they do not preclude it and possible evidence of overfitting can be found in partial dependence plots which do not conform to established response–driver relationships or are clearly driven by one or two observations. The relationship between CH<sub>4</sub>-D and littoral extent (Figure S3h) is an example where one or two observations seem to be driving a major feature of the partial dependence plot. Ultimately, the best way to minimize overfitting is to train the model with more data. This is not a trivial task in ecological systems where high spatial and temporal variability necessitate resource intensive sampling approaches, however. This highlights the importance of different research groups adopting comparable measurement approaches so that reports from unrelated studies can be combined for use in modeling

**Table 5**  
*Anthropogenic Methane Sources in Ohio*

Sector	CH <sub>4</sub> emission (Gg CH <sub>4</sub> y <sup>-1</sup> )
Waste	187.0
Enteric Fermentation	93.4
Petroleum and Natural Gas	29.6
Reservoir	21.3
Underground Coal Mines	14.3
Power Plants	6.4
Refineries	0.8
Ponds	0.3–1.5
Metals	0.3

*Note.* Reservoir emissions were estimated with this work and all other sources are for the year 2017. Enteric fermentation was taken from the Inventory of U.S. Greenhouse Gas Emissions and Sinks: 1990–2017 (Table A-182; U.S. Environmental Protection Agency, 2019b). All other sources were taken from the U.S. EPA's Greenhouse Gas Emissions from Large Facilities program (U.S. Environmental Protection Agency, 2019b).

efforts. We suggest that future studies of CH<sub>4</sub> emissions should include a robust statistical survey design, report system-scale emission rate estimates ( $\pm$  confidence interval) and employ measurement methods that integrate ebullition over a diurnal cycle.

#### 4.10. Upscaling and Extrapolating

We estimate that Ohio reservoirs emit 21.3 (13.3–30.8) Gg of CH<sub>4</sub> per year, which ranks as the fourth largest anthropogenic CH<sub>4</sub> source in the state following waste (mostly landfills), cattle enteric fermentation, and petroleum/natural gas production, processing, transmission, and storage (Table 5) (U.S. Environmental Protection Agency, 2019a, 2019b). These results reinforce previous reports that reservoirs are a significant anthropogenic CH<sub>4</sub> source in the United States (Beaulieu et al., 2014) and suggest that future work to improve emission estimates and identify mitigation strategies is merited.

While this study was conducted at a regional scale, GHG inventory reports assembled in accordance with United Nations Framework Convention on

Climate Change guidelines must be compiled at the national scale. To test the prediction accuracy of our CH<sub>4</sub>-T BRT model at the national scale, we predicted CH<sub>4</sub>-T for reservoirs in the U.S. Pacific Northwest (PNW) and Southeast (SE) for which published emission rates are available (Bevelhimer et al., 2016; Harrison et al., 2017) (Figure 6). The BRT poorly predicted CH<sub>4</sub>-T in these regions of the country, which is not surprising given differences in climate, geology, and land use among the PNW, SE, and our study area. It is also possible, however, that the poor prediction accuracy partly reflects model overfitting to our observations. A national scale prediction model should be trained with data collected at the national scale. To the best of our knowledge, the only published CH<sub>4</sub>-T rates for U.S. reservoirs are those for five reservoirs in the PNW (Harrison et al., 2017), six in the SE (Bevelhimer et al., 2016), and one reservoir in Ohio from our previous work (Beaulieu et al., 2014, 2016, 2018). While the data presented in this study will lead to a fourfold increase in the available literature data, there remain large portions of the United States where no measurements have been made. Given that CH<sub>4</sub>-T can vary over 4 orders of magnitude across reservoirs, we suggest that surveying reservoir CH<sub>4</sub>-T at the national-scale is a critical research need that must be addressed before an unbiased

estimate of U.S. reservoir CH<sub>4</sub> emissions can be made. The recent adoption of IPCC reporting guidelines for GHG emissions from reservoirs underscores the importance and timeliness of this issue (Lovelock et al., 2019).

## 5. Conclusions

We used statistically robust survey designs and standardized methods to measure diffusive and ebullitive emissions of CO<sub>2</sub> and CH<sub>4</sub> from 32 reservoirs spanning an agriculture to forested land use gradient, representing the largest such effort in the United States. We found that all reservoirs were a source of CH<sub>4</sub>, whereas over half were absorbing atmospheric CO<sub>2</sub>. The GWP of combined CO<sub>2</sub> and CH<sub>4</sub> emissions on a 100-year time horizon was positive in ~70% of sampled reservoirs, with CH<sub>4</sub> being the more important source of GWP in most.

Our work verifies previous reports that reservoir and watershed morphology influence lentic CO<sub>2</sub> and CH<sub>4</sub> dynamics. We also found that CH<sub>4</sub> emission rates were positively related to indices of allochthonous carbon inputs, whereas both CH<sub>4</sub> and CO<sub>2</sub> were related to measures of watershed agricultural activity.

An important finding of our work is that the prediction accuracy of CH<sub>4</sub> BRT models using readily available covariate information (i.e., NHDPlusV2 and derivative databases) was roughly equivalent to those that used information from field-based sampling efforts (i.e., water

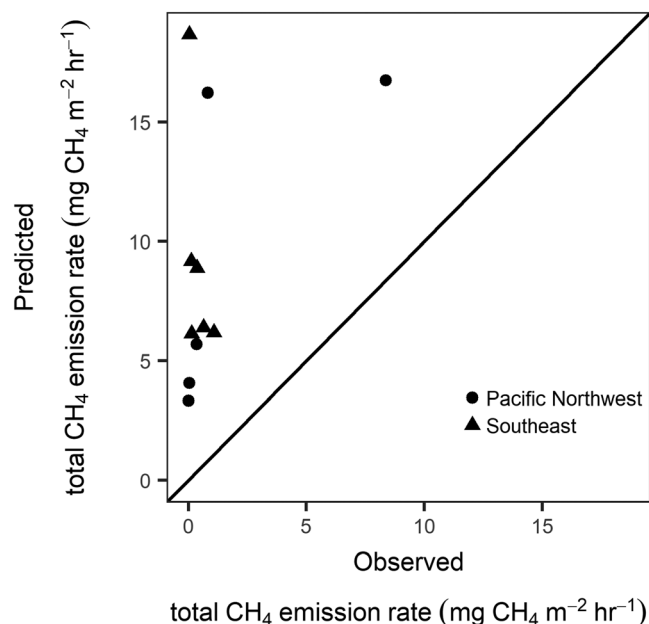


**Figure 6.** Predicted vs observed CH<sub>4</sub>-T for reservoirs in the U.S. Pacific Northwest and Southeast. Predictions were made using the BRT trained on field data collected in Ohio, Kentucky, and Indiana during this study.

chemistry and algal abundance), suggesting that CH<sub>4</sub> emissions from U.S. reservoirs can be estimated without the need for resource intensive field campaigns. This assumes that (1) models driven by national inputs will perform as well those using local inputs in other regions of the country and (2) comparable training data are available from a nationally distributed set of reservoirs. We therefore suggest that a critical next step in this research is to embark upon a national-scale survey of CH<sub>4</sub> and CO<sub>2</sub> emission rates from U.S. reservoirs.

## Data Availability Statement

Data supporting the conclusions presented in this paper are available in the FigShare data repository (<https://doi.org/10.6084/m9.figshare.8300531>). Data and code for generating the BRTs presented in this paper are available at the reservoirGbm repository at github (<http://doi.org/10.5281/zenodo.4062480>).

## Acknowledgments

The views expressed in this paper are those of the authors and do not necessarily reflect the views or policies of the U.S. Environmental Protection Agency. We thank the U.S. Army Corps of Engineers, U.S. Forest Service, Ohio Department of Natural Resources, Muskingum Watershed Conservancy District, Apple Valley Property Owners Association, RomeRock Association, Lake Mohawk Property Owners Association, and City of Akron, Ohio, for site access. Field, laboratory, and GIS support was provided by Pegasus Technical Services under contract EP-C-15-010. We thank the U.S. EPA Office of Air and Radiation for constructive discussions during this work.

## References

- Balmer, M. B., & Downing, J. A. (2011). Carbon dioxide concentrations in eutrophic lakes: Undersaturation implies atmospheric uptake. *Inland Waters*, 1(2), 125–132. <https://doi.org/10.5268/IW-1.2.366>
- Barros, N., Cole, J. J., Tranvik, L. J., Prairie, Y. T., Bastviken, D., Huszar, V. L. M., et al. (2011). Carbon emission from hydroelectric reservoirs linked to reservoir age and latitude. *Nature Geoscience*, 4(9), 593–596. <https://doi.org/10.1038/ngeo1211>
- Bastviken, D., Cole, J. J., Pace, M., & Tranvik, L. (2004). Methane emissions from lakes: Dependence of lake characteristics, two regional assessments, and a global estimate. *Global Biogeochemical Cycles*, 18, GB4009. <https://doi.org/10.1029/2004GB002238>
- Bastviken, D., Cole, J. J., Pace, M. L., & Van de Bogert, M. C. (2008). Fates of methane from different lake habitats: Connecting whole-lake budgets and CH<sub>4</sub> emissions. *Journal of Geophysical Research*, 113, G02024. <https://doi.org/10.1029/2007JG000608>
- Bastviken, D., Tranvik, L. J., Downing, J. A., Crill, P. M., & Enrich-Prast, A. (2011). Freshwater methane emissions offset the continental carbon sink. *Science*, 331(6013), 50. <https://doi.org/10.1126/science.1196808>
- Beaulieu, J. J., Balz, D. A., Birchfield, M. K., Harrison, J. A., Nietch, C. T., Platz, M. C., et al. (2018). Effects of an experimental water-level drawdown on methane emissions from a eutrophic reservoir. *Ecosystems*, 21(4), 657–674. <https://doi.org/10.1007/s10021-017-0176-2>
- Beaulieu, J. J., DelSontro, T., & Downing, J. A. (2019). Eutrophication will increase methane emissions from lakes and impoundments during the 21st century. *Nature Communications*, 10(1), 1375. <https://doi.org/10.1038/s41467-019-09100-5>
- Beaulieu, J. J., McManus, M. G., & Nietch, C. T. (2016). Estimates of reservoir methane emissions based on a spatially balanced probabilistic-survey. *Limnology and Oceanography*, 61, S27–S40. <https://doi.org/10.1002/lno.10284>
- Beaulieu, J. J., Smolenski, R. L., Nietch, C. T., Townsend-Small, A., & Elovitz, M. S. (2014). High methane emissions from a midlatitude reservoir draining an agricultural watershed. *Environmental Science & Technology*, 48(19), 11,100–11,108. <https://doi.org/10.1021/es501871g>
- Berberich, M. E., Beaulieu, J. J., Hamilton, T. L., Waldo, S., & Buffam, I. (2019). Spatial variability of sediment methane production and methanogen communities within a eutrophic reservoir: Importance of organic matter source and quantity. *Limnology and Oceanography*. <https://doi.org/10.1002/lno.11392>
- Bergier, I., Novo, E. M. L. M., Ramos, F. M., Mazzi, E. A., & Rasera, M. F. F. L. (2011). Carbon dioxide and methane fluxes in the littoral zone of a tropical savanna reservoir (Corumbá, Brazil). *Oecologia Australis*, 15(3), 666–681. <https://doi.org/10.4257/oeco.2011.1503.17>
- Bevelhimer, M. S., Stewart, A. J., Fortner, A. M., Phillips, J. R., & Mosher, J. J. (2016). CO<sub>2</sub> is dominant greenhouse gas emitted from six hydropower reservoirs in southeastern United States during peak summer emissions. *Watermark*, 8, 14. <https://doi.org/10.3390/w8010015>
- Bogren, K. (2001). *QuikChem(R) Method 10–115–01-4-E. Total phosphorus in manual persulfate digests*. Loveland, CO, USA: Lachat Instruments.
- Boudreau, B. P., Algar, C., Johnson, B. D., Croudace, I., Reed, A., Furukawa, Y., et al. (2005). Bubble growth and rise in soft sediments. *Geology*, 33(6), 517–520. <https://doi.org/10.1130/G21259.1>
- Breiman, L., Friedman, J. H., Olshen, R. A., & Stone, C. J. (1984). *Classification and Regression Trees*. Belmont, CA, USA: Wadsworth International Group.
- Carey, C. C., McClure, R. P., Doubek, J. P., Lofton, M. E., Ward, N. K., & Scott, D. T. (2017). Chaoborus spp. Transport CH<sub>4</sub> From the Sediments to the Surface Waters of a Eutrophic Reservoir, But Their Contribution to Water Column CH<sub>4</sub> Concentrations and Diffusive Efflux Is Minor. *Environmental Science & Technology*, 52(3), 1165–1173. <https://doi.org/10.1021/acs.est.7b04384>
- Chanton, J. P., Martens, C. S., & Kelley, C. A. (1989). Gas-transport from methane-saturated, tidal freshwater and wetland sediments. *Limnology and Oceanography*, 34(5), 807–819. <https://doi.org/10.4319/lo.1989.34.5.0807>
- Chen, Z. H., Ye, X. Q., & Huang, P. (2018). Estimating carbon dioxide (CO<sub>2</sub>) emissions from reservoirs using artificial neural networks. *Watermark*, 10. <https://doi.org/10.3390/w10010026>
- Clow, D. W., Stackpoole, S. M., Verdin, K. L., Butman, D. E., Zhu, Z., Krabbenhoft, D. P., & Striegl, R. G. (2015). Organic carbon burial in lakes and reservoirs of the conterminous United States. *Environmental Science & Technology*, 49(13), 7614–7622. <https://doi.org/10.1021/acs.est.5b00373>
- Cole, J. J., Caraco, N. F., Kling, G. W., & Kratz, T. K. (1994). Carbon dioxide supersaturation in the surface waters of lakes. *Science*, 265(5178), 1568–1570. <https://doi.org/10.1126/science.265.5178.1568>
- Cole, J. J., Prairie, Y. T., Caraco, N. F., McDowell, W. H., Tranvik, L. J., Striegl, R. G., et al. (2007). Plumbing the global carbon cycle: Integrating inland waters into the terrestrial carbon budget. *Ecosystems*, 10, 171–184. <https://doi.org/10.1007/s10021-006-9013-8>
- Davic, R. D., Eicher, D., & DeShon, J. (1997). *1996 Ohio Water Resource Inventory*. Columbus, Ohio: State Of Ohio Environmental Protection Agency.
- De Mello, N., Brighenti, L. S., Barbosa, F. A. R., Staehr, P. A., & Neto, J. F. B. (2018). Spatial variability of methane (CH<sub>4</sub>) ebullition in a tropical hypereutrophic reservoir: Silted areas as a bubble hot spot. *Lake and Reservoir Management*, 34(2), 105–114. <https://doi.org/10.1080/10402381.2017.1390018>



- Deemer, B. R., Harrison, J. A., Li, S. Y., Beaulieu, J. J., Delsontro, T., Barros, N., et al. (2016). Greenhouse gas emissions from reservoir water surfaces: A new global synthesis. *Bioscience*, 66(11), 949–964. <https://doi.org/10.1093/biosci/biw117>
- DelSontro, T., Beaulieu, J. J., & Downing, J. A. (2018). Greenhouse gas emissions from lakes and impoundments: Upscaling in the face of global change. *Limnology and Oceanography Letters*, 3(3), 64–75. <https://doi.org/10.1002/lol2.10073>
- DelSontro, T., Boutet, L., St-Pierre, A., del Giorgio, P. A., & Prairie, Y. T. (2016). Methane ebullition and diffusion from northern ponds and lakes regulated by the interaction between temperature and system productivity. *Limnology and Oceanography*, 61(S1), S62–S77. <https://doi.org/10.1002/lno.10335>
- DelSontro, T., Kunz, M. J., Kempter, T., Wuest, A., Wehrli, B., & Senn, D. B. (2011). Spatial heterogeneity of methane ebullition in a large tropical reservoir. *Environmental Science & Technology*, 45(23), 9866–9873. <https://doi.org/10.1021/es2005545>
- DelSontro, T., McGinnis, D. F., Sobek, S., Ostrovsky, I., & Wehrli, B. (2010). Extreme methane emissions from a Swiss hydropower reservoir: Contribution from bubbling sediments. *Environmental Science & Technology*, 44(7), 2419–2425. <https://doi.org/10.1021/es9031369>
- Demello, W. Z., & Hines, M. E. (1994). Application of static and dynamic enclosures for determining dimethyl sulfide and carbonyl sulfide exchange in *Sphagnum* peatlands: Implications for the magnitude and direction of flux. *Journal of Geophysical Research*, 99(D7), 14,601–14,607. <https://doi.org/10.1029/94JD01025>
- Deshmukh, C., Serça, D., Delon, C., Tardif, R., Demarty, M., Jarnot, C., et al. (2014). Physical controls on CH<sub>4</sub> emissions from a newly flooded subtropical freshwater hydroelectric reservoir: Nam Theun 2. *Biogeosciences*, 11(15), 4251–4269. <https://doi.org/10.5194/bg-11-4251-2014>
- Development Core Team, R. (2016). *R: A Language and Environment for Statistical Computing*. Vienna, Austria: R Foundation for Statistical Computing.
- Du, Q., Liu, H. Z., Liu, Y., Wang, L., Xu, L. J., Sun, J. H., & Xu, A. L. (2018). Factors controlling evaporation and the CO<sub>2</sub> flux over an open water lake in southwest of China on multiple temporal scales. *International Journal of Climatology*, 38(13), 4723–4739. <https://doi.org/10.1002/joc.5692>
- Efron, B. (1979). Bootstrap methods: Another look at the jackknife. *The Annals of Statistics*, 7(1), 1–26. <https://doi.org/10.1214/aos/1176344552>
- Elith, J., Leathwick, J. R., & Hastie, T. (2008). A working guide to boosted regression trees. *Journal of Animal Ecology*, 77(4), 802–813. <https://doi.org/10.1111/j.1365-2656.2008.01390.x>
- Elzhov, T. V., Mullen, K. M., Spiess, A.-N., & Bolker, B. (2016). *minpack.lm: R Interface to the Levenberg-Marquardt Nonlinear Least-Squares Algorithm Found in MINPACK, Plus Support for Bounds*. R package version (Vol. 1, pp. 2–1). Retrieved from <https://CRAN.R-project.org/package=minpack.lm>
- Erkkila, K. M., Ojala, A., Bastviken, D., Biermann, T., Heiskanen, J. J., Lindroth, A., et al. (2018). Methane and carbon dioxide fluxes over a lake: Comparison between eddy covariance, floating chambers and boundary layer method. *Biogeosciences*, 15(2), 429–445. <https://doi.org/10.5194/bg-15-429-2018>
- Fox, E. W., Hill, R. A., Leibowitz, S. G., Olsen, A. R., Thornbrugh, D. J., & Weber, M. H. (2017). Assessing the accuracy and stability of variable selection methods for random forest modeling in ecology. *Environmental Monitoring and Assessment*, 189(7), 316. <https://doi.org/10.1007/s10661-017-6025-0>
- Freeman, E. A., Moisen, G. G., Coulston, J. W., & Wilson, B. T. (2016). Random forests and stochastic gradient boosting for predicting tree canopy cover: Comparing tuning processes and model performance. *Canadian Journal of Forest Research*, 46(3), 323–339. <https://doi.org/10.1139/cjfr-2014-0562>
- Frolking, S., Roulet, N., & Fuglestedt, J. (2006). How northern peatlands influence the Earth's radiative budget: Sustained methane emission versus sustained carbon sequestration. *Journal of Geophysical Research*, 111, G01008. <https://doi.org/10.1029/2005JG000091>
- Gagnon, L., Belanger, C., & Uchiyama, Y. (2002). Life-cycle assessment of electricity generation options: The status of research in year 2001. *Energy Policy*, 30(14), 1267–1278. [https://doi.org/10.1016/S0301-4215\(02\)00088-5](https://doi.org/10.1016/S0301-4215(02)00088-5)
- Greenwell, B. M. (2017). pdp: An R package for constructing partial dependence plots. *R Journal*, 9(1), 421–436. <https://doi.org/10.32614/RJ-2017-016>
- Grinham, A., Dunbabin, M., Gale, D., & Udy, J. (2011). Quantification of ebullitive and diffusive methane release to atmosphere from a water storage. *Atmospheric Environment*, 45(39), 7166–7173. <https://doi.org/10.1016/j.atmosenv.2011.09.011>
- Hakanson, L. (1982). Lake bottom dynamics and morphometry—The dynamic ratio. *Water Resources Research*, 18(5), 1444–1450. <https://doi.org/10.1029/WR018i005p01444>
- Harrison, J. A., Deemer, B. R., Birchfield, M. K., & O'Malley, M. T. (2017). Reservoir water-level drawdowns accelerate and amplify methane emission. *Environmental Science & Technology*, 51(3), 1267–1277. <https://doi.org/10.1021/acs.est.6b03185>
- Hilgert, S., Fernandes, C. V. S., & Fuchs, S. (2019). Redistribution of methane emission hot spots under drawdown conditions. *Science of the Total Environment*, 646, 958–971. <https://doi.org/10.1016/j.scitotenv.2018.07.338>
- Hill, R. A., Weber, M. H., Debbout, R. M., Leibowitz, S. G., & Olsen, A. R. (2018). The Lake-Catchment (LakeCat) Dataset: Characterizing landscape features for lake basins within the conterminous USA. *Freshwater Science*, 37(2), 208–221. <https://doi.org/10.1086/697966>
- Hollister, J., & Stachelek, J. (2018). *Lakemorpho: Lake morphometry metrics*. R package version 1.1.1. <https://CRAN.R-project.org/package=lakemorpho>
- Hollister, J. W., Milstead, W. B., & Urrutia, M. A. (2011). Predicting maximum lake depth from surrounding topography. *PLoS ONE*, 6(9), e25764. <https://doi.org/10.1371/journal.pone.0025764>
- International Hydropower Association (2010). *GHG measurement guidelines for freshwater reservoirs*. London, UK: The International Hydropower Association (IHA).
- Jammet, M., Dengel, S., Kettner, E., Parmentier, F. J. W., Wik, M., Crill, P., & Friborg, T. (2017). Year-round CH<sub>4</sub> and CO<sub>2</sub> flux dynamics in two contrasting freshwater ecosystems of the subarctic. *Biogeosciences*, 14(22), 5189–5216. <https://doi.org/10.5194/bg-14-5189-2017>
- Jones, J. R., Obrecht, D. V., Graham, J. L., Balmer, M. B., Filstrup, C. T., & Downing, J. A. (2016). Seasonal patterns in carbon dioxide in 15 mid-continent (USA) reservoirs. *Inland Waters*, 6(2), 265–272. <https://doi.org/10.5268/IW-6.2.982>
- Kalff, J. (2002). *Limnology*. New Jersey, USA: Prentice Hall.
- Kemenes, A., Forsberg, B. R., & Melack, J. M. (2011). CO<sub>2</sub> emissions from a tropical hydroelectric reservoir (Balbina, Brazil). *Journal of Geophysical Research*, 116, G03004. <https://doi.org/10.1029/2010JG001465>
- Kincaid, T. M., & Olsen, A. R. (2015). *Spsurvey: Spatial Survey design and analysis*. R package version 3.0. Retrieved from <https://cran.r-project.org/web/packages/spsurvey/index.html>
- Knoll, L. B., Vanni, M. J., Renwick, W. H., Dittman, E. K., & Gephart, J. A. (2013). Temperate reservoirs are large carbon sinks and small CO<sub>2</sub> sources: Results from high-resolution carbon budgets. *Global Biogeochemical Cycles*, 27, 52–64. <https://doi.org/10.1002/gbc.20020>

- Knoll, L. B., Vanni, M. J., Renwick, W. H., & Kolli, S. (2014). Burial rates and stoichiometry of sedimentary carbon, nitrogen and phosphorus in Midwestern US reservoirs. *Freshwater Biology*, 59(11), 2342–2353. <https://doi.org/10.1111/fwb.12438>
- Koschorreck, M., Hentschel, I., & Boehrer, B. (2017). Oxygen ebullition from lakes. *Geophysical Research Letters*, 44, 9372–9378. <https://doi.org/10.1002/2017GL074591>
- Lapierre, J.-F., Seekell, D. A., Filstrup, C. T., Collins, S. M., Emi Fergus, C., Soranno, P. A., & Cheruvilil, K. S. (2017). Continental-scale variation in controls of summer CO<sub>2</sub> in United States lakes. *Journal of Geophysical Research: Biogeosciences*, 122, 875–885. <https://doi.org/10.1002/2016JG003525>
- Lazzarino, J. K., Bachmann, R. W., Hoyer, M. V., & Canfield, D. E. (2009). Carbon dioxide supersaturation in Florida lakes. *Hydrobiologia*, 627(1), 169–180. <https://doi.org/10.1007/s10750-009-9723-y>
- Li, S., & Bush, R. T. (2015). Revision of methane and carbon dioxide emissions from inland waters in India. *Global Change Biology*, 21(1), 6–8. <https://doi.org/10.1111/gcb.12705>
- Liden, R. (2013). *Interim Technical Note: Greenhouse Gases from Reservoirs Caused by Biochemical Processes*. World Bank, Water Unit, Transport, Water and ICT Department, Sustainable Development Vice Presidency. Water Papers are available online at <https://www.worldbank.org/water>
- Liu, H. P., Zhang, Q. Y., Katul, G. G., Cole, J. J., Chapin, F. S., & MacIntyre, S. (2016). Large CO<sub>2</sub> effluxes at night and during synoptic weather events significantly contribute to CO<sub>2</sub> emissions from a reservoir. *Environmental Research Letters*, 11(6), 064001. <https://doi.org/10.1088/1748-9326/11/6/064001>
- Lovelock, C. E., Evans, C., Barros, N., Prairie, Y. T., Alm, J., Bastviken, D., et al. (2019). Chapter 7—Wetlands. In *2019 refinement to the 2006 guidelines for National Greenhouse gas Inventories*. Retrieved from <https://www.ipcc.ch/report/2019-refinement-to-the-2006-ipcc-guidelines-for-national-greenhouse-gas-inventories/>
- MacIntyre, S., Wanninkhof, R., & Chanton, J. P. (1995). Trace gas exchange across the air-water interface in freshwater and coastal marine environments. In P. A. Matson & R. C. Harriss (Eds.), *Biogenic Trace Gases: Measuring Emissions from Soil and Water* (pp. 52–97). London: Blackwell Science.
- Madsen, T. V., & Sandjensen, K. (1991). Photosynthetic carbon assimilation in aquatic macrophytes. *Aquatic Botany*, 41(1–3), 5–40. [https://doi.org/10.1016/0304-3770\(91\)90037-6](https://doi.org/10.1016/0304-3770(91)90037-6)
- Maack, A., DelSontro, T., McGinnis, D. F., Fischer, H., Flury, S., Schmidt, M., et al. (2013). Sediment trapping by dams creates methane emission hot spots. *Environmental Science & Technology*, 47(15), 8130–8137. <https://doi.org/10.1021/es4003907>
- Maher, D. T., Drexler, M., Tait, D. R., Johnston, S. G., & Jeffrey, L. C. (2019). iAMES: An inexpensive, automated methane ebullition sensor. *Environmental Science & Technology*, 53(11), 6420–6426. <https://doi.org/10.1021/acs.est.9b01881>
- Mattson, M. D., & Likens, G. E. (1990). Air pressure and methane fluxes. *Nature*, 347(6295), 718–719. <https://doi.org/10.1038/347718b0>
- McGinnis, D. F., Greinert, J., Artemov, Y., Beaubien, S. E., & Wüest, A. (2006). Fate of rising methane bubbles in stratified waters: How much methane reaches the atmosphere? *Journal of Geophysical Research*, 111, C09007. <https://doi.org/10.1029/2005JC003183>
- McKay, L., Bondelid, T., Dewald, T., Johnson, J., Moore, R., & Rea, A. (2018). *NHDPlus Version 2: User Guide (Data Model Version 2.1)*. Retrieved from <https://www.epa.gov/waterdata/get-nhdplus-national-hydrography-dataset-plus-data>
- Mosher, J. J., Fortner, A. M., Phillips, J. R., Bevelhimer, M. S., Stewart, A. J., & Troia, M. J. (2015). Spatial and temporal correlates of greenhouse gas diffusion from a hydropower reservoir in the southern United States. *Watermark*, 7(11), 5910–5927. <https://doi.org/10.3390/w7115910>
- Musenze, R. S., Grinham, A., Werner, U., Gale, D., Sturm, K., Udy, J., & Yuan, Z. (2014). Assessing the spatial and temporal variability of diffusive methane and nitrous oxide emissions from subtropical freshwater reservoirs. *Environmental Science & Technology*, 48(24), 14,499–14,507. <https://doi.org/10.1021/es505324h>
- Nakagawa, F., Yoshida, N., Nojiri, Y., & Makarov, V. N. (2002). Production of methane from allassesin eastern Siberia: Implications from its C-14 and stable isotopic compositions. *Global Biogeochemical Cycles*, 16(3), 14–1–14–15. <https://doi.org/10.1029/2000GB001384>
- Natchimuthu, S., Selvam, B. P., & Bastviken, D. (2014). Influence of weather variables on methane and carbon dioxide flux from a shallow pond. *Biogeochemistry*, 119(1–3), 403–413. <https://doi.org/10.1007/s10533-014-9976-z>
- Natchimuthu, S., Sundgren, I., Galfalk, M., Klemetsson, L., Crill, P., Danielsson, A., & Bastviken, D. (2016). Spatio-temporal variability of lake CH<sub>4</sub> fluxes and its influence on annual whole lake emission estimates. *Limnology and Oceanography*, 61(S1), S13–S26. <https://doi.org/10.1002/lno.10222>
- Olsen, A. R., Kincaid, T. M., & Payton, Q. (2012). Spatially balanced survey designs for natural resources. In R. A. Gitzen, J. J. Millspaugh, A. B. Cooper, D. S. Licht (Eds.), *Design and Analysis of Long-Term Ecological Monitoring Studies* (pp. 126–150). United Kingdom: Cambridge University Press. <https://doi.org/10.1017/CBO9781139022422.010>
- Papale, D., & Valentini, A. (2003). A new assessment of European forests carbon exchanges by eddy fluxes and artificial neural network spatialization. *Global Change Biology*, 9(4), 525–535. <https://doi.org/10.1046/j.1365-2486.2003.00609.x>
- Podgrajsek, E., Sahlee, E., & Rutgersson, A. (2014). Diurnal cycle of lake methane flux. *Journal of Geophysical Research: Biogeosciences*, 119, 236–248. <https://doi.org/10.1002/2013JG002327>
- Prairie, Y. T., Alm, J., Beaulieu, J., Barros, N., Battin, T., Cole, J., et al. (2017). Greenhouse gas emissions from freshwater reservoirs: What does the atmosphere see? *Ecosystems*. <https://doi.org/10.1007/s10021-017-0198-9>
- Prairie, Y. T., Alm, J., Harby, A., Mercier-Blais, S., & Nahas, R. (2017). The GHG Reservoir Tool (G-res) User guide, UNESCO/IHA research project on the GHG status of freshwater reservoirs. Version 1.12. Joint publication of the UNESCO Chair in Global Environmental Change and the International Hydropower Association, 38 pp. Retrieved from <https://www.hydropower.org/gres>
- Rasilo, T., Prairie, Y. T., & Del Giorgio, P. A. (2015). Large-scale patterns in summer diffusive CH<sub>4</sub> fluxes across boreal lakes, and contribution to diffusive C emissions. *Global Change Biology*, 21(3), 1124–1139. <https://doi.org/10.1111/gcb.12741>
- Reis, P. C., & Barbosa, F. A. (2014). Diurnal sampling reveals significant variation in CO<sub>2</sub> emission from a tropical productive lake. *Brazilian Journal of Biology*, 74(3 suppl 1), S113–S119. <https://doi.org/10.1590/1519-6984.01713>
- Ridgeway, G. (2017). *gbm: Generalized boosted regression models. R package version 2.1.3*. Retrieved from <https://CRAN.R-project.org/package=gbm>
- Rinta, P., Bastviken, D., Schilder, J., Van Hardenbroek, M., Stötter, T., & Heiri, O. (2016). Higher late summer methane emission from central than northern European lakes. *Journal of Limnology*, 76. <https://doi.org/10.4081/jlimnol.2016.1475>
- Rudd, J. W. M., Harris, R., Kelly, C. A., & Hecky, R. E. (1993). Are hydroelectric reservoirs significant sources of greenhouse gases. *Ambio*, 22, 246–248.
- Rusak, J. A., Tanentzap, A. J., Klug, J. L., Rose, K. C., Hendricks, S. P., Jennings, E., et al. (2018). *Wind and trophic status explain within and among-lake variability of algal biomass* (Vol. 3, pp. 409–418). <https://doi.org/10.1002/lol2.10093>

